Pharmacological Research 138 (2018) 43–56

Contents lists available at ScienceDirect

Pharmacological Research

journal homepage: www.elsevier.com/locate/yphrs

Regulation of ER-mitochondria contacts by Parkin via Mfn2

Valentina Basso[a,b], Elena Marchesan[b], Caterina Peggion[c], Joy Chakraborty[a,b], Sophia von Stockum[b], Marta Giacomello[a], Denis Ottolini[a], Valentina Debattisti[d], Federico Caicci[a], Elisabetta Tasca[b], Valentina Pegoraro[b], Corrado Angelini[b], Angelo Antonini[e], Alessandro Bertoli[c], Marisa Brini[a], Elena Ziviani[a,b,*]

[a] Department of Biology, University of Padova, Padova, Italy
[b] Fondazione Ospedale San Camillo, IRCCS, Lido di Venezia, Venezia, Italy
[c] Department of Biomedical Science (DSB), University of Padova, Padova, Italy
[d] MitoCare Center for Mitochondrial Imaging Research and Diagnostics, Department of Pathology, Anatomy and Cell Biology, Thomas Jefferson University, Philadelphia, PA, USA
[e] Department of Neuroscience, University of Padova, Padova, Italy

ARTICLE INFO

Keywords:
Mitochondria
Parkinson's disease
ER-mitochondria tethering
Mitofusin
Parkin
PINK1
Ubiquitination
ER-mitochondria synthetic tether
Drosophila model of PD

ABSTRACT

Parkin, an E3 ubiquitin ligase and a Parkinson's disease (PD) related gene, translocates to impaired mitochondria and drives their elimination via autophagy, a process known as mitophagy. Mitochondrial pro-fusion protein Mitofusins (Mfn1 and Mfn2) were found to be a target for Parkin mediated ubiquitination. Mfns are transmembrane GTPase embedded in the outer membrane of mitochondria, which are required on adjacent mitochondria to mediate fusion. In mammals, Mfn2 also forms complexes that are capable of tethering mitochondria to endoplasmic reticulum (ER), a structural feature essential for mitochondrial energy metabolism, calcium (Ca^{2+}) transfer between the organelles and Ca^{2+} dependent cell death. Despite its fundamental physiological role, the molecular mechanisms that control ER-mitochondria cross talk are obscure. Ubiquitination has recently emerged as a powerful tool to modulate protein function, via regulation of protein subcellular localization and protein ability to interact with other proteins. Ubiquitination is also a reversible mechanism, which can be actively controlled by opposing ubiquitination-deubiquitination events. In this work we found that in Parkin deficient cells and *parkin* mutant human fibroblasts, the tether between ER and mitochondria is decreased. We identified the site of Parkin dependent ubiquitination and showed that the non-ubiquitinatable Mfn2 mutant fails to restore ER-mitochondria physical and functional interaction. Finally, we took advantage of an established *in vivo* model of PD to demonstrate that manipulation of ER-mitochondria tethering by expressing an ER-mitochondria synthetic linker is sufficient to rescue the locomotor deficit associated to an *in vivo Drosophila* model of PD.

1. Introduction

Parkinson's disease (PD) is the second most common neurodegenerative disease, for which there is no cure. Although the exact cause of most cases is unknown, both environmental and genetic factors are implicated in the onset of the disease. In the last few years, a number of genes have been identified, which cause inherited PD and account for ~10% of PD cases [1]. Some of these genes encodes for proteins that are either expressed in the mitochondria or targeted to the mitochondria upon stressful condition. Indeed, mitochondrial dysfunction is strongly implicated in the aetiology of the disease and impaired mitochondria are found in animal and cell models of PD [2].

Mitochondria form a tubular, reticulated network which shape is controlled by opposing fusion and fission events [3]. The Mitofusins 1 and 2 (Mfn1 and Mfn2) are conserved dynamin-like GTPases, composed of a large cytosolic GTPase domain, an HR1 domain, a double transmembrane domain embedded in the outer mitochondrial membrane (OMM) and a second HR2 domain (HR2) [4]. Mfn1 mediate mitochondrial fusion of OMM in coordination with OPA1, which mediates the fusion of IMM [5,6]. While Mfn1 seems primarily involved in organellar docking and fusion, Mfn2 is enriched at contact sites between ER and mitochondria called MERC (mitochondria-ER contact sites) where it regulates organelles tethering [7–10]. MERCs are sites of dynamic physical and functional interaction that regulate phospholipid

* Corresponding author at: Department of Biology, University of Padova, Padova, Italy.
E-mail address: elena.ziviani@unipd.it (E. Ziviani).

https://doi.org/10.1016/j.phrs.2018.09.006
Received 2 March 2018; Received in revised form 4 July 2018; Accepted 6 September 2018
Available online 13 September 2018

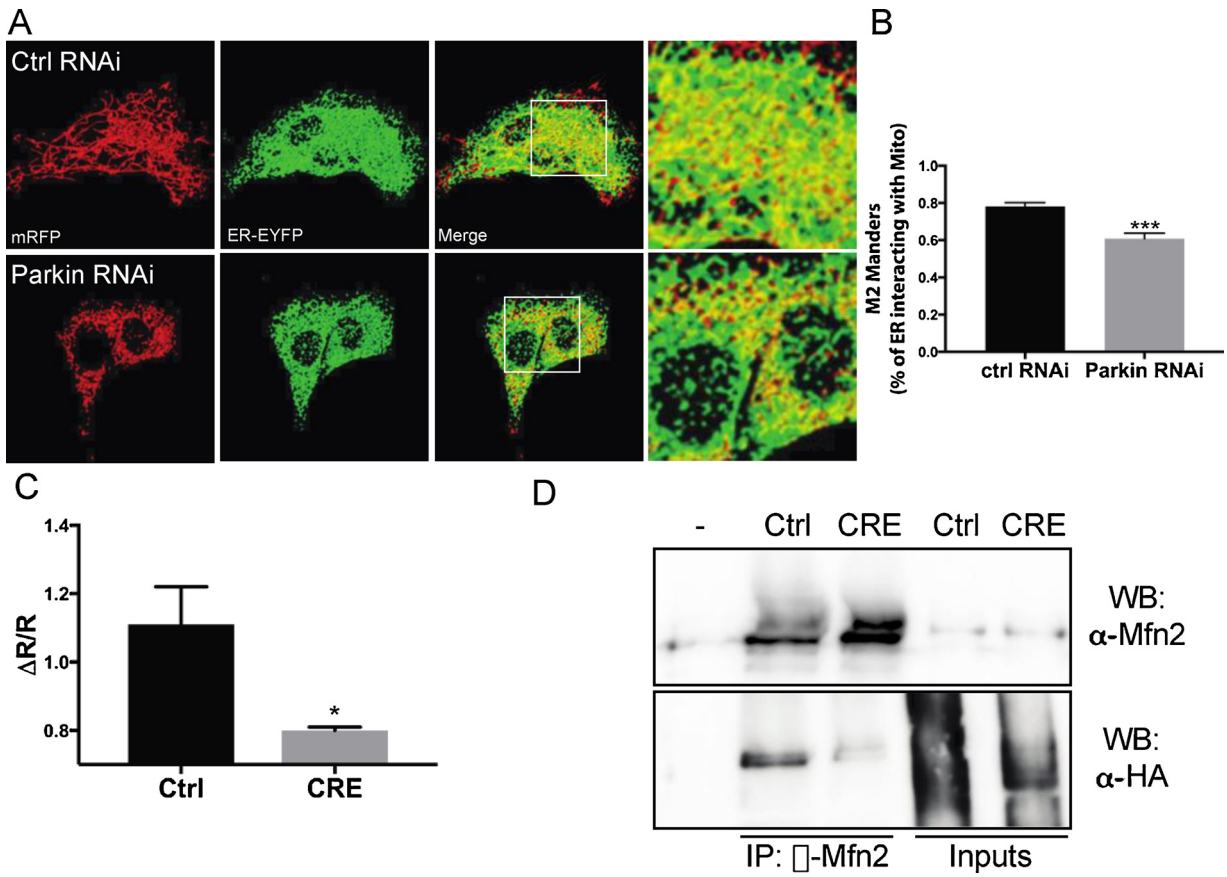

Fig. 1. Parkin regulates ER-mitochondria contacts.
(A) MEFs were transfected with either Parkin siRNA or Scamble siRNA (Ctrl RNAi). Mitochondria and ER were probed using organelles targeted fluorescence probes (mRFP and ER-YFP respectively). The overlap between red and green fluorescence (yellow spots) represents area of organelle tethering. Panels on the right show enlarged views of the boxed areas. B) Graph bar indicates mean ± SEM of percentage of ER co-localizing with mitochondria (degree of tethering) by using Mander's coefficient of co-localization upon volume-rendered 3D reconstruction of *z*-axis stacks of confocal images (n = 8, 12–15 cells per experiment). Unpaired Two-tailed *t*-test P value = 0.0005 (C) Parkin$^{Flx/Flx}$ MEFs were transfected with pcDNA 3.1 (Ctrl) or pcDNA 3.1-Cre (CRE) and in combination with the FEMP probe. FRET ratio (ΔR/R) was calculated as described in materials and methods. Graph bar indicates mean ± SEM. n = 4; Unpaired Two-tailed *t*-test P value = 0.0485. (D) Parkin$^{Flx/Flx}$ MEF cells were transfected with pcDNA 3.1-CRE or empty vector, Mfn2 (Myc-Mfn2) and HA-Ub and subjected to immunoprecipitation (IP) of Mfn2 using α-Mfn2 antibody (Abcam). WB analysis was performed with antibodies α-Mfn2 (Abnova) or α-HA (cell signaling) on the pulled down samples. (-) identify samples incubated without antibody (negative control). Inputs represent 10% of the protein lysates and IP eluate 100% of the protein lysates (For interpretation of the references to colour in this figure legend, the reader is referred to the web version of this article.).

exchange and synthesis, Ca^{2+} homeostasis, autophagosome formation and mitochondria fission [11–,1–13]. Recently it became clear that ER-mitochondria contacts are altered under pathological conditions. In particular, a number of proteins which mutations are linked to the onset of familiar cases of PD, such as Alpha-synuclein, PINK1, Parkin and DJ1, have been localised at the MERCs, and are able to modulate ER-mitochondria cross talk *in vitro* [13–,14,15,16,17].

Parkin, an E3-ubiquitin ligase mutated in familiar PD is selectively recruited to dysfunctional mitochondria and promotes their elimination via autophagy, a process known as mitophagy [18]. PINK1, a protein kinase, also a PD related gene, is required for Parkin recruitment and stress induced mitophagy [19]. In 2008 Poole et al. showed a strong genetic interaction between PINK1/Parkin pathway and mitochondrial fission and fusion machinery. By using the fruitfly *Drosophila*, they found that PINK1 or Parkin mutant (knock out) phenotypes, including locomotor defects, loss of dopaminergic neurons and degeneration of the muscle of the thorax, is suppressed by inhibiting mitochondrial fusion or by promoting mitochondrial fission [20]. This genetic interaction was explained by the subsequent discovery that Parkin physically interacts with and ubiquitinates Marf (dMfn), fly homologue of mammalian Mitofusins, to control its steady state levels [19]. This work was followed by others that showed that in several model systems, including HeLa cells [21] and human neuroblastoma cells SH-SY5Y [22], Parkin selectively ubiquitinates mammalian Mfn1 and Mfn2. Accordingly, lack of Parkin (or PINK1 which operates upstream Parkin in the same pathway) [23–26] results in increased amount of the steady state levels of dMfn and a reduction of dMfn ubiquitination forms [19].

In this work we show that a post-translational modification (PTM), e.g. a Parkin dependent ubiquitination, plays an indispensable role in the formation of ER-mitochondria contacts sites via Mfn2. Moreover, we demonstrate that *in vivo* manipulation of ER-mitochondria tethering by expressing an ER-mitochondria synthetic linker is sufficient to rescue the locomotor deficits associated to an *in vivo Drosophila* model of PD.

2. Results

2.1. Parkin regulates ER-mitochondria contacts

In S2R+ *Drosophila* cells overexpression of Flag tagged dMfn allows the identification of four bands by western blotting (WB). As previously shown, the smaller molecular weight band (~90KDa) corresponds to unmodified dMfn whereas the upper bands (~100KDa, 130KDa and 140KDa) correspond to monoubiquitinated and multiubiquitinated forms of dMFN, respectively [19]. A similar pattern of ubiquitination was also previously described for Mfn2 in Hela cells [21], human neuroblastoma cells SH-SY5Y [22] and for the yeast Mfn homologue,

fuzzy onions (Fzo1) [27]. This pattern of ubiquitination is PINK1/Parkin dependent. Accordingly, in the absence of PINK1 or Parkin, steady state levels of dMfn are increased and the pattern of ubiquitination is abolished [19]. Considering that dMfn in the fruit fly includes both promotion of fusion and ER-mitochondria crosstalk [28] and the role of Mfn2 in ER-mitochondria tethering [7–10,29], we investigated the degree of tethering between ER and mitochondria upon Parkin downregulation, i.e. in a condition where dMfn ubiquitination is impaired. Volume rendered 3D reconstruction of *z*-axis stacks of confocal images of fluorescent-tagged mitochondria and ER has been previously used to measure contact sites between the two organelles [12]. We transfected S2R + fly cells with expression vectors encoding mitochondrial and endoplasmic reticulum fluorescent marker (mDsRed and ER-GFP respectively) and upon treatment with Ctrl or Parkin dsRNA to specifically knock down Parkin. We then measured the degree of tethering by using Mander's coefficient of co-localization upon volume-rendered 3D reconstruction of *z*-axis stacks of confocal images. In such 3D reconstruction, the overlap between red and green fluorescence (yellow spots) represents area of organelle tethering. We found a clear decrease in ER-mitochondria interaction in Parkin downregulating cells (Supplementary Fig. 1A–B). To consolidate these data, we performed electron microscopy (EM) analysis on control and *parkin* downregulating cells and measured the average distance between mitochondria and the juxtaposing ER. We found a significant increase in ER-mitochondria distance (i.e. MERCs width) in *parkin* deficient S2R + cells (Supplementary Fig. 1C–D) and an overall decrease in the average number of ER-mitochondria contacts per mitochondria (Supplementary Fig. 1E) compared to control cells. To validate our findings, we performed the same measurement in a different cell type. MEFs cells, treated with scramble (Ctrl) or Parkin siRNA, were transfected with mitochondrial and endoplasmic reticulum fluorescent marker (mRFP and ER-YFP respectively). We observed a clear reduction in ER-mitochondria contacts in Parkin downregulating cells (Fig. 1A–B), as previously showed [14]. To consolidate these data, we also measured ER-mitochondria proximity by using a modified FRET-based indicator of ER-mitochondria proximity named FEMP [29]. This sensor is targeted to the mitochondrial outer membrane (OMM) (targeting sequence mAKAP1 connected to YPF fluorescent protein) and ER (targeting sequence Sac1 connected to CFP fluorescent protein) and contains a self-leaving Tav2 A peptide, which undergoes autocleavage releasing YFP and CFP. This sensor is designed to guarantee almost equimolar expression of YFP on the mitochondrial outer membrane (OMM) and of the Cyan fluorescent protein (CFP) on the ER surface. FRET intensity is inversely proportional to the distance between the two fluorophores, thus allowing a quantitative measurement of organelles proximity. In the FEMP probe, OMM and ER targeting sequence are coupled with the two components of the FKBP-FRP heterodimerization system that allows covalent linkage between ER and mitochondria upon rapamycin administration. ER-mitochondria juxtaposition can therefore be correlated to FRET intensity and rapamycin treatment allows heterodimerization between adjacent FKBP and FRB domains to maximize energy transfer. We analyzed FRET ratio changes in MEFs coming from conditional Parkin KO mice in which Parkin expression can be deleted upon expression of Cre recombinase by recombining loxP sites *ad hoc* inserted in exon 7 ($Parkin^{Flx/Flx}$ mice) [30,31]. Transfection of MEFs with pcDNA 3.1-Cre leads to an obvious decrease in Parkin mRNA as compared to pcDNA 3.1 transfected cells (Supplementary Fig. 1F). We transfected $Parkin^{Flx/Flx}$ MEFs with pcDNA 3.1 (CTRL) or pcDNA 3.1-Cre (CRE) and in combination with the FEMP probe. We measured a decrease in the FEMP FRET ratio in Parkin downregulating cells further sustaining the knowledge that ER-mitochondria tethering is reduced in Parkin downregulating conditions (Fig. 1C). We thought to extend these data and investigate the pattern of Mfn2 ubiquitination in these conditions. To do that, we transfected $Parkin^{Flx/Flx}$ MEFs with empty vector, pcDNA 3.1 (CTRL), or pcDNA 3.1-Cre (CRE) and in combination with Myc-tagged form of Mfn2 (MFN2) and hemagglutinin (HA)-tagged ubiquitin (HA-Ub). Western blotting analysis of Mfn2 by using anti Mfn2 antibody revealed a single band of the predicted size of Mfn2 (~86 KDa) in the total lysate. Western blotting analysis of the total lysate with antibody against HA revealed the expected smear of ubiquitinated forms, which was partially decreased upon Parkin deletion. To assess whether Mfn2 is ubiquitin modified, we performed coimmunoprecipitation analysis against HA-Ub. Immunoprecipitates of Mfn2 were prepared by using anti Mfn2 antibody and WB analysis was performed with antibody against HA on the pulled down samples. Following enrichment by immunoprecipitation, we observed a clear reduction of Mfn2-Ub (Fig. 1D). Thus, also in a mammalian cell type, impaired Mfn2 ubiquitination correlates to defective ER-mitochondria tethering.

These results sustain the hypothesis that aberrant ER-mitochondria interaction occurs in the absence of *parkin,* a condition that leads to impaired Mfn2 ubiquitination.

2.2. CMT type 2A disease-associated MFN mutants are not ubiquitinated and are incompetent in promoting ER-mitochondria interaction

Ablation of *Mfn2* in mice is embryonically lethal and *Mfn2* mutations in humans are associated with the onset of Charcot-Marie-Tooth neuropathy type 2A (CMT2A), an hereditary axonal peripheral neuropathy with patients developing early and severe motor disabilities that in the most severe cases constrict them to wheelchair [32,33]. The most frequent mutation in Mfn2 found in CMT2 A patients, R94Q, cannot restore ER-mitochondria contacts in *Mfn2* KO MEFs [8]. We looked at the pattern of ubiquitination in S2R + *Drosophila* cells upon expression of Flag-tagged form of MFN^{R94Q} mutant and two additional CMT type 2 A disease-associated MFN mutations (P251 A and R280H, respectively) and we found a complete loss of the ubiquitinated MFN forms in S2R + *Drosophila* cells (Supplementary Fig. 2). To examine whether this was also the case in mammalian cells, we looked at the pattern of Mfn2 ubiquitination in *Mfn2* KO MEFs transiently reconstituted with either wild type Mfn2 or mutants $Mfn2^{P251A}$ and $Mfn2^{R280H}$. Western blotting analysis of Mfn2 by using anti Mfn2 antibody revealed a single band of the predicted size of Mfn2 (~86 KDa) (Fig. 2A). Immunoprecipitates of wt Mfn2, $Mfn2^{P251A}$ and $Mfn2^{R280H}$ were prepared by using anti Mfn2 antibody and WB analysis was performed with antibody against Ubiquitin on the pulled down samples to identify ubiquitinated forms of Mfn2. We observed a clear reduction of Mfn2-Ub in all CMT type 2 A disease-associated Mfn2 mutants (Fig. 2A). Remarkably, we observed a reduction in ER-mitochondria contacts in *Mfn2* KO MEFs reconstituted with $Mfn2^{P251A}$ or $Mfn2^{R280H}$ as compared to wt Mfn2 (Fig. 2B–C).

These results further sustain the intriguing hypothesis that ubiquitination of Mfn2, rather than its steady state levels, is an essential prerequisite for ER-mitochondria tethering.

2.3. Ubiquitination of Lysine 416 in the HR1 Mfn2 domain control physical and functional ER-mitochondria interaction

Our results indirectly suggest that lack of MFN ubiquitination correlates to impaired ER-mitochondria interaction. With that in mind, we conducted a bioinformatics study to identify the potential Mfn2 site that could be ubiquitinated by Parkin. Mfn1 and Mfn2 are anchored at the outer mitochondrial membrane and have N- and C-terminal domains that protrude into the cytosol. At the N-terminus, there is a GTP binding domain, followed by a hydrophobic heptad repeat region (HR1) and a transmembrane domain (TM), which allows anchorage to the outer membrane. At the C-terminal, there is a second hydrophobic heptad repeat (HR2) [4]. This protein structure is highly conserved between different species [4], although an interesting work recently challenged this model, providing functional evidences that mammalian Mfns are single- spanning outer membrane proteins with an N_{out}-C_{in} orientation [34]. Nevertheless, a number of publications reported an almost identical pattern of ubiquitination for yeast homologue *fuzzy onion* (fzo1)

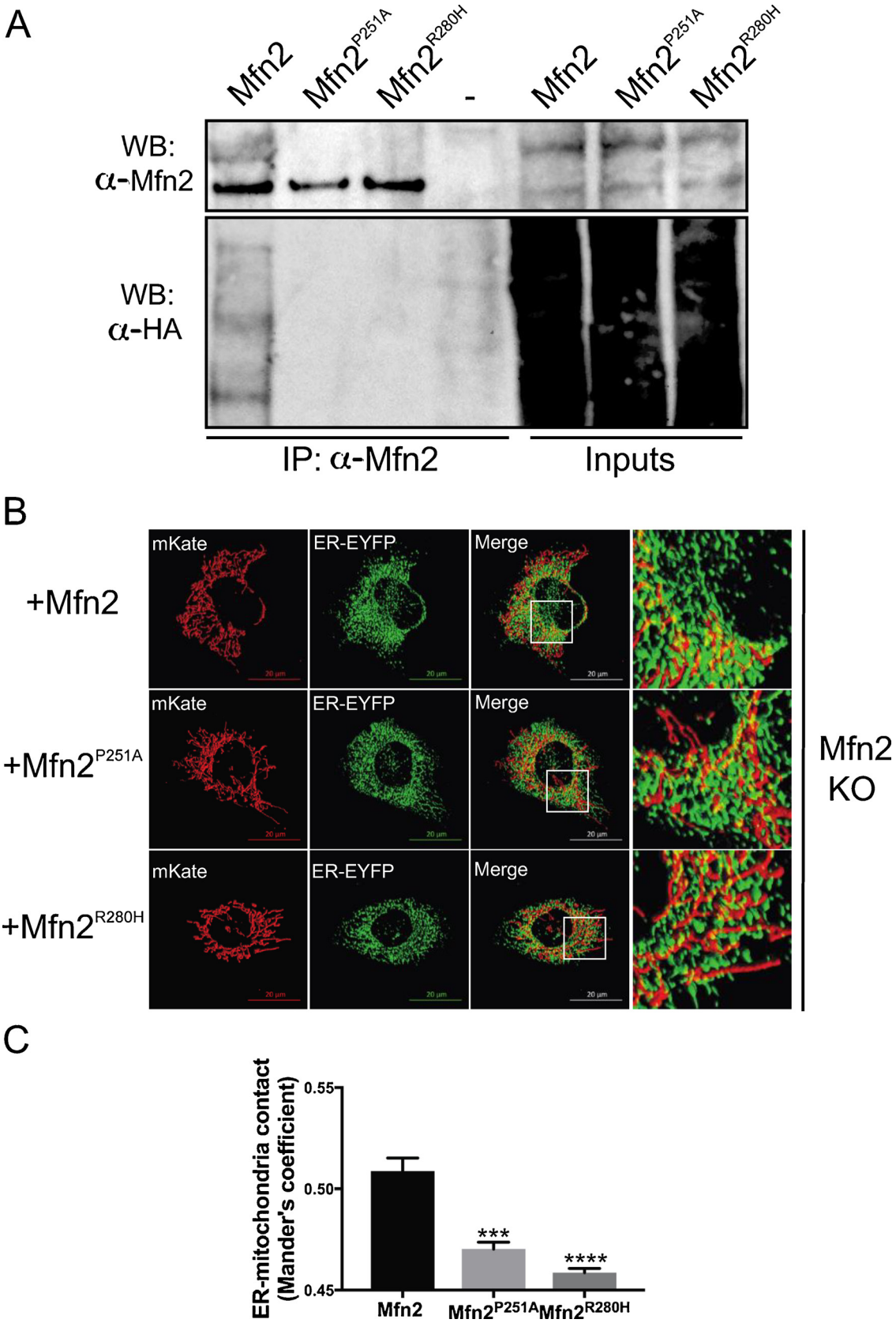

(caption on next page)

Fig. 2. CMT type 2 A disease-associated MFN mutants are not ubiquitinated and are incompetent in promoting ER-mitochondria interaction.
(A) *Mfn2* KO MEFs were transfected with the indicated plasmids and in combination with HA-Ub. After 24 h, cells were lysed and subjected to immunoprecipitation (IP) by α-Mfn2 antibody (Abcam). Western blotting analysis was performed by using α-HA antibody and α-Mfn2 (Abnova) on the pulled down samples. Inputs represent 10% of the protein lysates and IP eluate 100% of the protein lysates. (B) *Mfn2* KO MEFs were transfected the indicated plasmids. Mitochondria and ER were probed using organelles targeted fluorescence probes (mitoKate and ER-YFP respectively). Yellow spots represent area of organelle tethering. Panels on the right show enlarged views of the boxed areas. The scale bar is 20 μm. (C) Graph bar indicates mean ± SEM of percentage of ER co-localizing with mitochondria (degree of tethering) by using Mander's coefficient of co-localization upon volume-rendered 3D reconstruction of z-axis stacks of confocal images of cells transfected as indicated. (n = 4, 15 cells per experiment). One way ANOVA, p value < 0.0001. Dunnett's multiple comparison test (Mfn2 vs $Mfn2^{P251A}$ p value = 0.0003; Mfn2 vs $Mfn2^{R280H}$ p value = 0.0001) (For interpretation of the references to colour in this figure legend, the reader is referred to the web version of this article.).

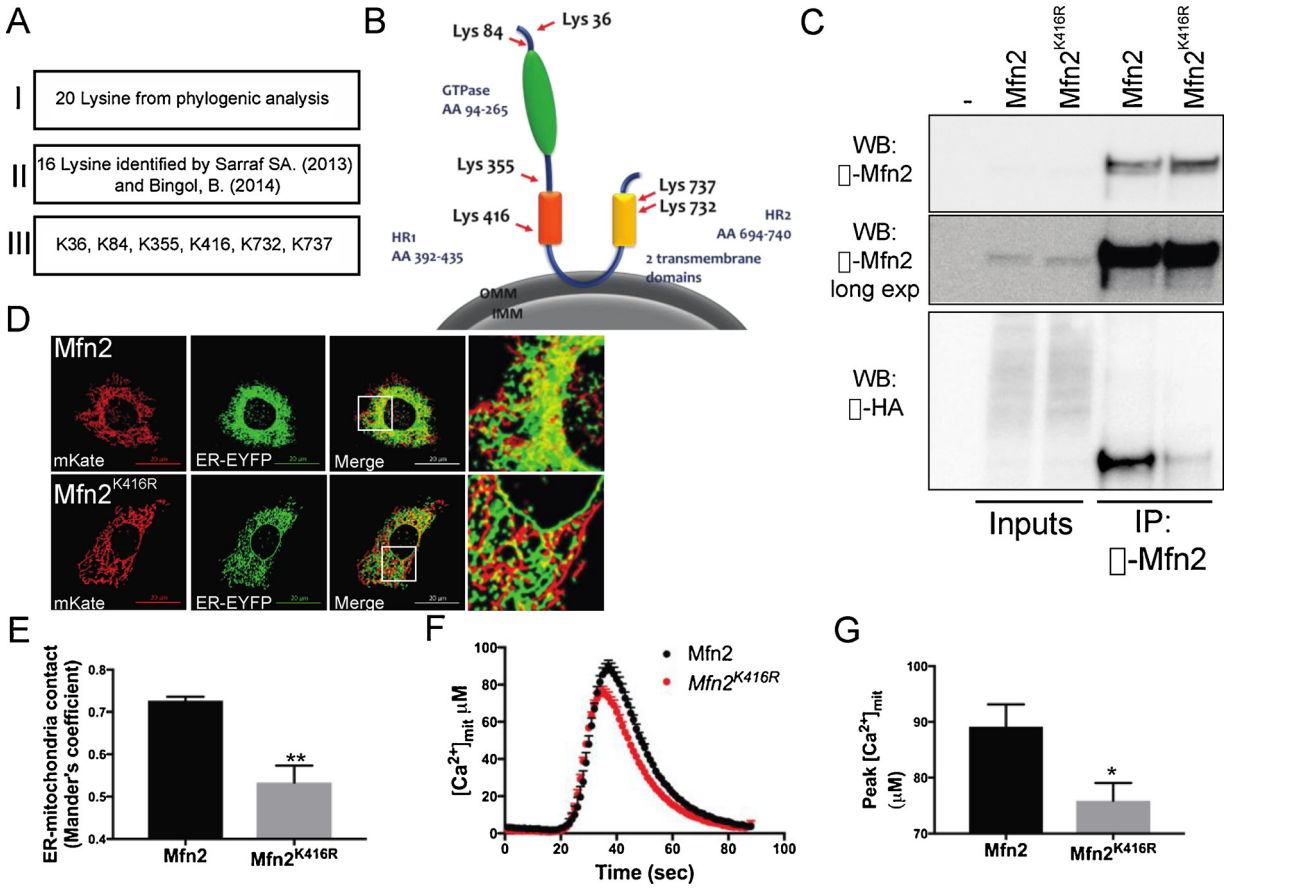

Fig. 3. Ubiquitination of Lysine 416 in the HR1 Mfn2 domain control physical and functional ER-mitochondria interaction.
(A) Panel shows a diagram of the *modus operandi* to identify the lysine residues (Lys, K) that are ubiquitinated by Parkin (see text) (B) Schematic representation of Mfn2 protein based on [4]. Residues K36 and K84 are located at the N-terminal of the protein, before the GTPase domain. Residue K355 is positioned between the GTPase and HR1 domain. Residue K416 is within the HR1 domain. Residues K732 and K737 are in the HR2 domain. C) *Mfn2* KO MEFs were transfected with the indicated plasmids and in combination with HA-Ub and lysed after 24 h. Protein lysates were subjected to IP by using α-Mfn2 antibody. WB analysis on the pulled down sample was performed by using α-Mfn2 or α-HA antibody. (-) identify samples incubated without antibody (negative control). Inputs and IP eluate represent 2% and 100% of the protein lysates, respectively. (D) *Mfn2* KO MEFs were transfected with the indicated plasmids. Mitochondria and ER were probed using organelles targeted fluorescence probes (mitoKate and ER-YFP respectively). Yellow spots represents area of organelle tethering. Panels on the right show enlarged views of the boxed areas. The scale bar is 20 μm. (E) Graph bar indicates mean ± SEM of percentage of ER co-localizing with mitochondria (degree of tethering) by using Mander's coefficient of co-localization upon volume-rendered 3D reconstruction of z-axis stacks of confocal images (n = 4, 15 cells per experiment. Unpaired Two-tailed *t*-test p value = 0.0029). (F) Mean ± SEM of $[Ca^{2+}]_{mit}$ from nine independent experiments where *Mfn2* KO MEFs were transfected with the indicated plasmids and mtAEQ. (G) Average ± SEM of peak $[Ca^{2+}]_{mit}$ in nine independent experiments performed as in G (Unpaired Two-tailed *t*-test p value = 0.0186) (For interpretation of the references to colour in this figure legend, the reader is referred to the web version of this article.).

[27,35], fly homologue Marf/dMfn [19] and human Mfn2 [21,35,36]. We therefore thought it was reasonable to hypothesis that the site of ubiquitination may be evolutionary conserved among species. Indeed, multiple sequence alignments using MultAlin revealed a high degree of homology between human, mouse and dMfn protein sequence. This phylogenic analysis identified twenty Lysine residues (K) that are conserved between these species (arrowheads Supplementary Fig. 3A–B). Two independent studies also identified by using a mass spectrometry approach, a number of Lysine residues that are ubiquitinated upon Parkin overexpression [37,38]. We matched the residues identified by these works with ours, and we identified six Lysine residues that are likely to represent good candidates for Parkin-dependent ubiquitination of Mfn2 (Fig. 3A). As illustrated, K36 and K84 are located at the N-terminal of the protein, before the GTPase domain, K355 is positioned between the GTPase and HR1 domain, K416 is within the HR1 domain and K732 and K737 are in the HR2 domain (Fig. 3B). We proceeded by generating non-ubiquitinatable mutants for each domain, and in this case for K36, K416 and K737 by substituting Lysine with Arginine (R), a common procedure to impair ubiquitination [39]. We expressed Flag-tagged mutants $dMfn^{K36R}$, $dMfn^{K416R}$ and $dMfn^{K737R}$ in

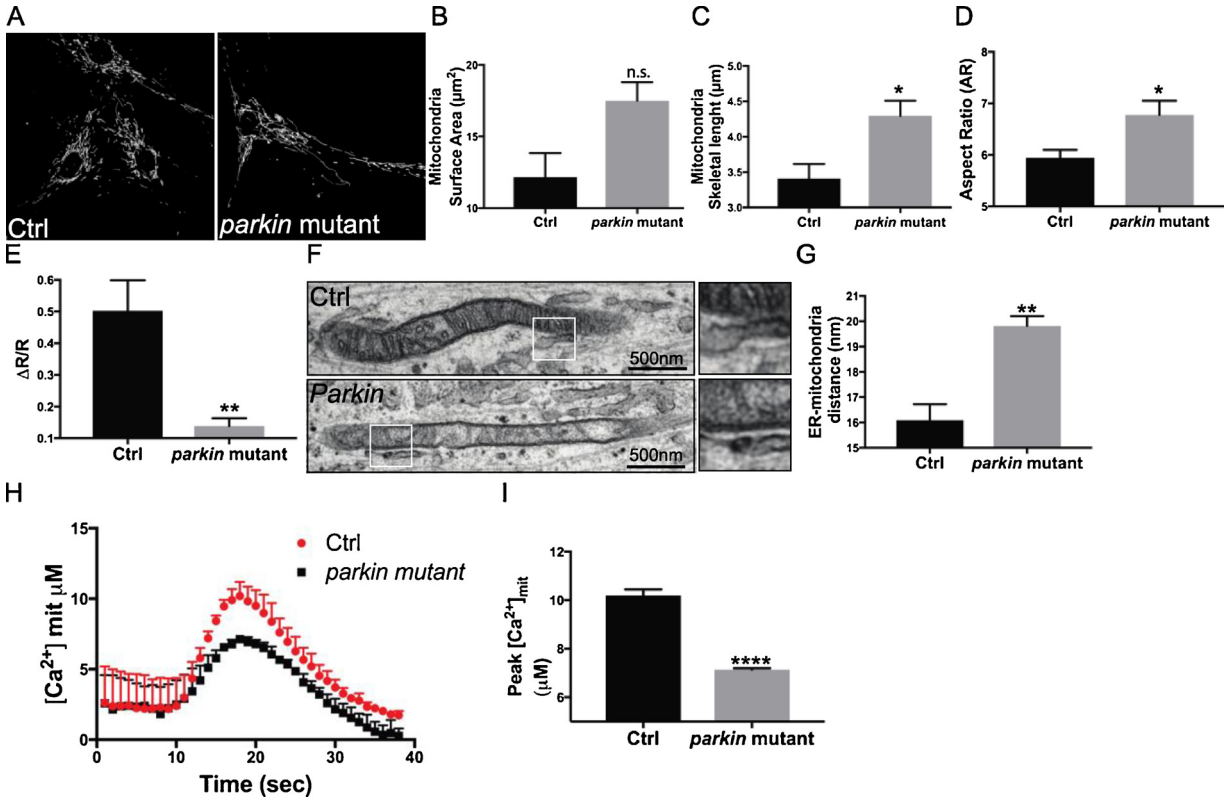

Fig. 4. ER-mitochondria physical and functional interaction is impaired in *parkin* mutant fibroblasts.
(A) Representative images of confocal acquisition of human fibroblast of the indicated genotypes generated from skin biopsy loaded with 1 μ M of Tetramethylrhodamine methyl ester (TMRM). The 60 *z*-axis images separated by 0.2 μm were analysis using Volocity 6.3 software, to obtain analysis of the mitochondrial volume, surface area (B) (unpaired Two-tailed *t*-test p value = 0.0655), skeletal length (C) (unpaired Two-tailed *t*-test P value = 0.0401) and the aspect ratio (D) (unpaired Two-tailed *t*-test P value = 0.05) calculated as described in materials and methods. Graph bars represents mean ± SEM of n = 3 replicates. (E) Human fibroblast of the indicated genotypes were infected with the FEMP probe. FRET ratio (ΔR/R) was calculated as described in materials and methods. Graph bar indicates mean ± SEM. n = 3; unpaired Two-tailed *t*-test p value = 0.0065 (F) Representative TEM images of human fibroblast of the indicated genotypes. (G) Mean ± SEM of mitochondria-ER distance calculated in four independent experiments as in F. Unpaired Two-tailed *t*-test p value = 0.0074. n = 3. (H) Mean ± SEM of $[Ca^{2+}]_{mit}$ from four independent experiments of human fibroblast of the indicated genotypes, transfected with mtAEQ. Cells were perfused with a mixture of 0.1 μM ATP and 0.1 μM histamine. (I) Average ± SEM of peak $[Ca^{2+}]_{mit}$ in four independent experiments performed as in H. Unpaired Two-tailed *t*-test p value < 0.0001.

S2R+ *Drosophila* cells. Western blotting analysis of dMfn by using anti Flag antibody revealed a single band of the predicted size of unmodified dMfn (~90 KDa) and a number of higher molecular weight bands which corresponds to mono and poly ubiquitinated forms of dMfn, as previously described [19]. Interestingly, expression of non-ubiquitinatable mutant $dMfn^{K416R}$ failed to reproduce the predicted pattern of ubiquitination (Supplementary Fig. 3C). Confocal microscopy analysis confirmed the mitochondrial subcellular localization of mutant $dMfn^{K416R}$ (Supplementary Fig. 3D), which indicated that impaired ubiquitination could not be due to misplacement of the protein. We next analysed the pattern of ubiquitination of non-uniquitinatable mutant $Mfn2^{K416R}$ in MEFs. To do that, we transfected *Mfn2* KO MEFs with Myc-tagged form of wild type Mfn2 (Mfn2) or the non-ubiquitinatable mutant ($Mfn2^{K416R}$) and HA-Ub. Western blotting analysis of wild type Mfn2 and $Mfn2^{K416R}$ by using anti Mfn2 antibody revealed a single band of the predicted size of Mfn2 (~86 KDa). To assess whether Mfn2 was ubiquitin modified, immunoprecipitates of Mfn2 were prepared by using anti Mfn2 antibody and WB analysis was performed with antibody against HA on the pulled down samples. We observed a clear reduction of ubiquitinated forms in the non-ubiquitinatable mutant $Mfn2^{K416R}$ (Fig. 3C), further supporting the notion that K416 in the HR1 Mfn2 domain is a genuine Parkin-dependent Mfn2 ubiquitination site.

To directly demonstrate the physiological significance of impaired MFN ubiquitination and ER-mitochondria miscommunication, we next evaluated whether non-ubiquitinatable mutant $Mfn2^{K416R}$ is incompetent in promoting ER-mitochondria physical and functional interaction. To this aim, we expressed $Mfn2^{K416R}$ or wild type Mfn2 in *Mfn2* KO MEFs and measured ER-mitochondria physical interaction as previously described. Remarkably, we observed a reduction in ER-mitochondria contacts in *Mfn2* KO MEFs reconstituted with non-ubiquitinatable mutant $Mfn2^{K416R}$ (Fig. 3D–E). To evaluate the functional counterpart of ER-mitochondria physical interaction, we next measured ER-mitochondria Ca^{2+} transfer in *Mfn2* KO MEFs reconstituted with non-ubiquitinatable mutant $Mfn2^{K416R}$. In *Mfn2* KO cells expressing mutant $Mfn2^{K416R}$, mitochondrial Ca^{2+} uptake following ATP-generated $InsP_3$ signaling is significantly diminished (Fig. 3F–G).

Thus, ubiquitination of Lysine 416 in the HR1 Mfn2 domain controls physical and functional ER-mitochondria interaction.

2.4. ER-mitochondria physical and functional interaction is impaired in parkin mutant fibroblasts

Our results strongly indicate a causal link between impaired ubiquitination of Mfn2 and physical and functional ER-mitochondria miscommunication, specifically in the context of Parkin deficiency. Although the exact cause for dopaminergic neurons loss in PD patients is unknown, these cells are highly susceptible to perturbations in Ca^{2+} homeostasis and lipid transfer, both affected upon impaired ER-mitochondrial juxtaposition [40,41]. An elegant study has shown that the

vulnerability of dopaminergic neurons depends on their reliance on a specific subtype of voltage dependent L-type Ca^{2+} channels that require Ca^{2+} to maintain their autonomous pacemaking activity and which expression is age dependent. Blocking these channels has a neuroprotective effect because it allows neurons to "rejuvenile" and go back to a Ca^{2+} independent mechanism to generate their pacemaking activity [42]. This work highlighted the importance of age-dependent Ca^{2+} homeostasis regulation for the survival of dopaminergic neurons, and led us to the intriguing hypothesis that ER-mitochondria miscommunication might also add to the disease onset. With that in mind, we conducted a study to analyse mitochondria morphology and ER-mitochondria physical and functional interaction in a characterized clinical case of PD patient associated *with a parkin*-mutant. We used four sets of techniques, namely live cell confocal imaging of organelle morphology, electron microscopy, FRET based measurement of ER-mitochondria physical proximity and Aequorin based measurement of ER-mitochondria Ca^{2+} transfer, to assess the shape of mitochondria, and ER-mitochondria physical and functional interaction in fibroblasts coming from skin biopsy of *parkin* patient with compound heterozygous (R275 W and exon 3 deletion) *parkin* mutations. We started by investigating mitochondrial morphology in primary fibroblasts culture coming from skin biopsy of *parkin* patient and age matched control. Primary fibroblasts were loaded with membrane potential independent mitochondrial dye Mitotracker red (Molecular Probes) that allows qualitative *in vivo* imaging assessment of mitochondria morphology by confocal microscopy (Fig. 4A). Mitochondria morphology was analysed by Volocity software (PerkinElmer) upon three-dimensional (3D) reconstruction and volume rendering of confocal stacks. Mitochondrial surface area (Fig. 4B), skeletal length (Fig. 4C), diameter (Supplementary Fig. 4A), aspect ratio (AR, Fig. 4D) and volume (Supplementary Fig. 4B) were measured from three independent clones coming from *parkin* patient skin biopsy and age matched control. We found increased mitochondrial surface area as well as mitochondrial skeletal length and AR in cells coming from *parkin* mutant patient compared to control (Fig. 4B–D), clearly indicating altered mitochondrial morphology in primary fibroblasts deriving from *parkin* patient. We next measured ER-mitochondria proximity by using the FEMP probe as previously done [29]. *Parkin* patient cells expressing the FEMP probe measured a decrease in the FEMP FRET ratio compared to control cells, supporting the knowledge that ER-mitochondria distance is increased in *parkin* patient (Fig. 4E). To extend these observations we compared our previous finding with electron microscopy (EM) analysis of control and *parkin* fibroblasts. We measured the average distance between mitochondria and the juxtaposing ER and we found a significant increase in ER-mitochondria distance (i.e. MERCs width) in *parkin* deficient patient cells (Fig. 4F–G). We finally evaluated the functional counterpart of ER-mitochondria structural alteration of *parkin* patient cells, by looking at ER-mitochondria Ca^{2+} transfer. To this aim, we infected primary fibroblasts with mitochondrially targeted Ca^{2+} sensor Aequorin, and we measured mitochondrial Ca^{2+} uptake following ATP/histamine-generated $InsP_3$ signalling. We found a significant decrease in mitochondrial Ca^{2+} transient upon ATP/histamine stimulation in *parkin* fibroblasts, (Fig. 4H–I), whether cytosolic Ca^{2+} transient was unaffected (Supplementary Fig. 4C–D). These results are indicative of aberrant ER-mitochondria Ca^{2+} flux in *parkin* patient cells and functionally correlates to defective ER-mitochondria physical interaction.

2.5. Expression of ER-mitochondria synthetic tether rescues the locomotor defect of a Drosophila model of Parkinson's disease

One of the most important functions of ER-mitochondria cross talk includes coordinating Ca^{2+} transfer and elegant studies have shown that artificial tether between the ER and mitochondria can be used to modulate Ca^{2+} transfer [43,44]. Starting from the rational that normalization of interorganelle contacts and ER-mitochondria Ca^{2+} transfer could be beneficial in PD models of aberrant Ca^{2+} homeostasis, we investigated the effect of expressing an ER-mitochondria synthetic linker in *Drosophila* PINK1 KO, a well-established *in vivo* model of PD that is deficient for Parkin function [19,45]. This is also presumably a good *in vivo* model of aberrant Ca^{2+} homeostasis, since a number of studies have previously shown impaired Ca^{2+} handling in cellular models lacking PINK1 [46,47]. We generated two *Drosophila* transgenic lines that allow visualising *in vivo* in the adult wing ER-mitochondria contacts through expression of a synthetic tether construct driven by a neuron-specific driver. The construct was created by Csordás et al. [43] and encodes monomeric red fluorescent protein (mRFP) fused to the OMM-targeting sequence (MTS) of mAKAP1 at the N-terminus and fused to the ER-targeting sequence (ERTS) of yUBC6 at the C-terminus (Supplementary Fig. 5A). We cloned the construct for the synthetic linker into a fly vector and generated two "tethering" lines by random insertion in a wild type *(white1118)* background under expression of the GAL4-UAS system. These lines expressed mild (TM, Tether Mild) to high (TH, Tether High) levels of the tethering construct. We expressed the TM "tethering" line in wild type $(white1118)^{-}$ and PINK1 mutant (KO) flies ($PINK1^{B9}$). To assess that the construct was appropriately expressed, and to visualize *ex vivo* ER-mitochondrial contacts in the fly, we took advantage of a recently described model, which allows imaging of sensory neurons in the translucent fly wing [48]. We fixed flies of the desired age in PFA, detached the wing and measured ER-mitochondria contact sites by imaging at confocal microscope of the red fluorescent signal in the L1 vein neuron bundle. In order to activate neuronal expression of the UAS tether lines we crossed these lines with nSyb-Gal4 (neuronal Synaptobrevin) expressing flies. We observed well-defined and easily quantifiable red fluorescent spots throughout the L1 vein that perfectly matched the pattern seen when expressing only mito-GFP or ER-GFP in the wing neurons (Supplementary Fig. 5B). Interestingly, we observed a reduced expression of the tethering probe (i.e. reduction in the RFP signal) in PINK1 KO flies (Fig. 5A–B), indicative of a previously described impairment in the mitochondrial protein import machinery of the PINK1 deficient flies [49]. Next we used a well-established locomotor assay to evaluate *in vivo* the physiological relevance of expressing the synthetic ER-mitochondria linker. In such assay, 10 flies for each strain were collected in a vertical plastic tube positioned with a line drawn at 6 cm from the bottom of the tube and under a light source. After tapping the flies to the bottom of the tube, the flies that successfully climbed above the mark after 10 s were counted (Fig. 5C). As already reported, $PINK1^{B9}$ mutant (PINK1 KO) flies performed poorly in the climbing assay compared to wild type (Ctrl) flies (Fig. 5D). Remarkably, climbing performance of PINK1 KO flies was significantly improved upon expression of the synthetic ER-mitochondria linker TM (Fig. 5D), sustaining the hypothesis that *in vivo* genetic normalization of ER-mitochondria tethering is beneficial in ameliorating the locomotor impairment associated to PINK1 deficiency. Of note, expression of the TH (tether high) synthetic tethering construct resulted lethal in wild type but not in PINK1 KO background, where it did not ameliorate the climbing performance of PINK1 flies (Fig. 5E) further corroborating the hypothesis that fine tuning ER-mitochondria interaction by expression of the synthetic linker has physiological implications *in vivo*. Intriguingly, TH expression did not impact eggs to pupae viability (Fig. 5F), but impaired adults/pupae ratio (Fig. 5G) indicating an age dependent lethality that occurs when pupae become adults.

3. Discussion

Parkin, a protein which mutations have been linked to the onset of a rare autosomal recessive form of familiar PD, is an E3 ubiquitin ligase that belongs to the Ring-between-RING (RBR) type of E3 ubiquitin ligases, also known as RING/HECT hybrids [50]. By mediating the covalent attachment of the highly conserved 76-amino acid protein ubiquitin on target proteins, Parkin controls a fundamental post-translational modification (PTM) that is required for proteasome-dependent protein degradation. Parkin is predominantly localized in the

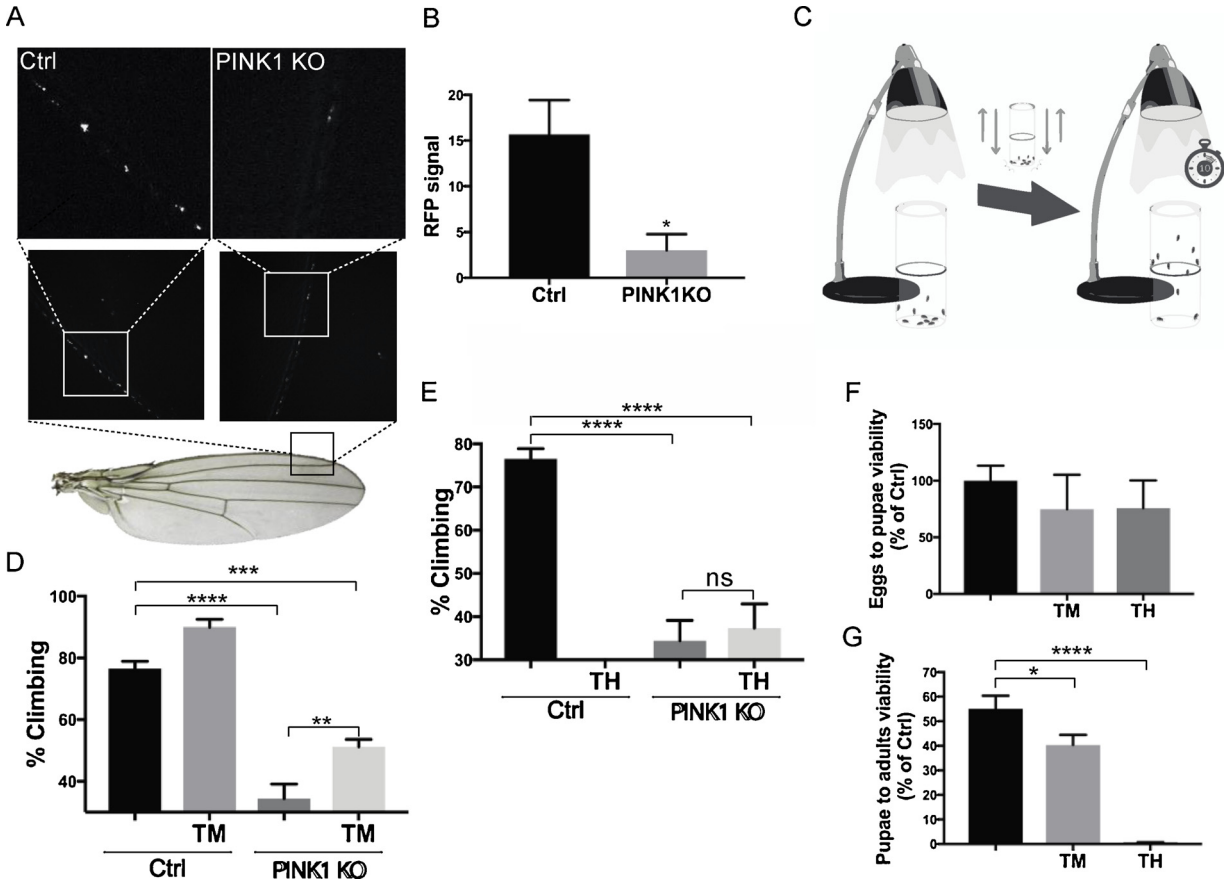

Fig. 5. Expression of ER-mitochondria synthetic tether rescues the locomotor defect of a *Drosophila* model of Parkinson's Disease.
(A) Representative images of TM (tether mild) "tethering" line in wild type (*white1118*)$^{-}$ and PINK1 mutant (KO) background (PINK1^{B9}). The down panels shown enlarge views of the 150 nm length along the L1 vein neural bundle from the intersection of the L2 vein to proximal side of the wing flies. (B) RFP signal in the wing of flies of the indicated genotype was quantified as described in materials and methods. Graph bar indicates mean ± SEM of the number of RFP spots. n = 3. Unpaired Two-tailed *t*-test P value = 0.0381 (C) Schematic representation of the climbing assay. 10 flies were put into a tube in a dark room. A light was put on the top of the tube. After tapping the flies at the bottom of the tube, the number of flies that successfully climbed above the 6-cm mark after 10 s was noted. (D) Graph bars represents means ± SEM of percentage (%) of climbing of flies of the indicated genotype. TM (tether mild) "tethering" line in wild type (*white1118*)- and PINK1 mutant (KO) backgound (PINK1B9). n = 5, 10 flies per experiment. One way ANOVA, p value < 0.0001. One way ANOVA, p value < 0.0001. Tukey's multiple comparison test (Ctrl vs Ctrl + TM p value = 0.0377; Ctrl vs PINK1 KO p value < 0.0001; Ctrl vs PINK1 KO + TM, p value = 0.0001; Ctrl + TM vs PINK1 KO, p value < 0.0001; Ctrl + TM vs PINK1 KO + TM, p value < 0.0001, PINK1 KO vs PINK1 KO + TM, p = 0.0055). (E) Graph bar represents means ± SEM of percentage (%) of climbing of flies of the indicated genotype. TH (tether high) "tethering" line in wild type (*white1118*)- and PINK1 mutant (KO) background (PINK1^{B9}) n = 5, 10 flies per experiment. One way ANOVA, p value < 0.0001. Tukey's multiple comparison test (Ctrl vs Ctrl + TH p value < 0.0001; Ctrl vs PINK1 KO p value < 0.0001; Ctrl vs PINK1 KO + TH, p value < 0.0001; Ctrl + TH vs PINK1 KO, p value < 0.0001; Ctrl + TH vs PINK1 KO + TH, p value < 0.0001, PINK1 KO vs PINK1 KO + TH, p value = 0.9293). (F) Graph bar indicates means ± SEM of egg to pupae ratio (% of Ctrl) calculated as described in materials and methods. (n = 3). (G) Graph bar indicates means ± SEM of adults to pupae ratio. n = 3. One way ANOVA, p value < 0.0001. Tukey's multiple comparison test (Ctrl vs TM p value = 0.0284; Ctrl vs TH p value < 0.0001; TM vs TH, p value < 0.0001).

cytosol, but it can translocate to depolarized mitochondria where it promotes polyubiquitination of outer mitochondrial membrane resident proteins, which is a prerequisite for mitochondria quality control or mitophagy, a well characterized cellular process that leads to the elimination of a selective subset of damaged mitochondria via autophagy [18]. In a number of cellular models, Parkin promotes the ubiquitination of Marf/dMfn (fly homologue of mammalian Mitofusins) [19] and both Mitofusin 1 (Mfn1) and Mitofusin 2 (Mfn2) [21,22]. Ubiquitination of Mitofusins leads to proteasome- and p97-dependent degradation of the proteins [21]. However, recent studies reported proteosome-independent-mediated ubiquitinations by Parkin, which do not result in degradative ubiquitination. For example, in 2006 two groups independently observed that Parkin catalyzes the formation of multiple monoubiquitination *in vitro* [51,52]. Additional study propounded that Parkin activation results in the formation of K63-linked ubiquitin chains, which does not results in decreased levels of the target protein [53]. Similarly it was demonstrated that Parkin can form linear ubiquitination of NF-κB essential modulator (NEMO) causing the activation of NF-κB pro-survival pathway [50]. All these observations suggest that Parkin may act like a multi-functions ubiquitin protein ligase capable of both mediating degradative ubiquitination (proteosomal or autophagy-dependent degradation) [19,21,22,54,55], as well as regulative ubiquitination (non degradative ubiquitination) [50–,51,52,53,56–,57,58,59]. Not surprisingly, Parkin exists in an inactive state that resembles that of a coiled snake and its activity is finely regulated and repressed by mechanisms of autoinhibition under normal conditions [60,61].

Parkin targets Mitofusins, large GTPase proteins that are required on adjacent mitochondria to promote tethering and fusion of the outer mitochondria membrane. In mammals Mfn2 also regulates ER-mitochondrial tethering [7–10,29]. ER-mitochondria physical interaction is a structural feature that is indispensable for Ca^{2+} cross talk, phospholipid biosynthesis, autophagosome formation, DRP1 mediated mitochondrial fission and a number of additional physiological signaling pathways that are essential for cell survival [12,13,40,62–65]. Starting from the observation that Parkin downregulation in MEFs results in

decreased ubiquitinatinated forms of Mfn2, as also observed in *Drosophila* cells [19], HeLa and human neuroblastoma cells [21,22], we addressed the effect of Parkin downregulation on ER-mitochondria physical and functional communication. By using four independent approaches (namely live cell confocal imaging of organelle morphology, electron microscopy, FRET based measurement of ER-mitochondria physical proximity and Aequorin based measurement of ER-mitochondria Ca^{2+} transfer) we showed that Parkin downregulation induced a decrease in ER-mitochondria physical and functional interaction, confirming previous findings [14]. We also found that Charcot Marie Tooth type 2 A disease-associate Mfn2 mutants, P251 A and P280H, failed to be ubiquitinated and are incompetent in promoting ER-mitochondria interaction. These observations prompted us to investigate whether ubiquitination of Mfn2 might operate as a functional PTM that is required on juxtaposing ER-mitochondria to promote organelle physical interaction. To prove this hypothesis, we engaged on a bioinformatics and a mass spectrometry-based analysis to identify the site/s of Parkin dependent ubiquitination on Mfn2 molecule. We identified lysine 416 localized in the HR1 domain of Mfn2. We generated a non-ubiquitinatable K416 mutant, which failed to be ubiquitinated and was also incompetent in promoting ER-mitochondria physical interaction. The non ubiquitinatable mutant not only altered physical contacts formation, but also impaired the functionality of ER-mitochondria communication, reducing mitochondrial Ca^{2+} uptake upon treatment that generated ER Ca^{2+}relase. Of note, no changes in the steady state levels of non ubiquitinatable mutant $Mfn2^{K416R}$ was observed, supporting the intriguing hypothesis that ubiquitination of Mfn2 on a specific lysine residue rather then Mfn2 steady state levels is crucial for proper ER-mitochondria interaction.

Aberrations in ER-mitochondria juxtaposition have been described in cellular models of a number of neurodegenerative diseases, including Parkinson's disease [14–16,66]. One of the most important functions of ER-mitochondria cross talk includes coordinating Ca^{2+} transfer and a number of studies have also shown impaired Ca^{2+} homeostasis in cellular models lacking PINK1 or Parkin [14,46,47,67–69]. Although it is not clear why dopaminergic neurons specifically degenerate in PD, it is tempting to hypothesize that this could be due to impaired Ca^{2+} cross talk at ER-mitochondria interface. Supporting this hypothesis we found that primary fibroblasts coming from skin biopsy of *parkin* patient display structural and functional ER-mitochondria miscommunication. Starting from the rational that normalization of ER-mitochondria Ca^{2+} transfer could be beneficial, we investigated the effect of expressing an ER-mitochondria synthetic linker in a well-established *in vivo Drosophila* model of PINK1 loss of function. PINK1 mutant (KO) flies have a very obvious phenotype characterized by male sterility, degeneration of thorax muscle, degeneration of dopaminergic neurons, locomotor defects, reduction in lifespan and mitochondrial dysfunction [23–25]. We demonstrated that expression of the mild tether (TM) induced a significantly improvement in the climbing performance of PINK1 KO flies, supporting the notion that ER-mitochondria cross talk normalization could be effective in ameliorating some of the phenotypes that are associated to PD neurodegeneration, and may hold substantial therapeutic implication for this disorder.

Altogether, these results led us to envision a model where Parkin dependent ubiquitination of Mfn2 is required on healthy mitochondria to mediate ER-mitochondria crosstalk (Fig. 6(a) upper representation). This model does not exclude the existence of a parallel stress induced pathways (like those generated by intoxicating substances), which promotes Parkin-dependent ubiquitination of Mfn2, and additional OMM resident proteins, to promote mitophagy (Fig. 6(b) lower representation).

4. Materials and methods

4.1. Cell culture

Drosophila S2R + cells grow at 25 °C without CO_2, as semi-adherent monolayer in tissue culture flasks. The complete medium for SR2 + cells is Schneider's *Drosophila* Medium (Gibco) containing 10% heat-inactivated fetal bovine serum (FBS). Transfection was performed using Effectene Transfection Reagent (QIAGEN) following manufacturer instruction. 5 h after the transfection medium was removed and change with fresh medium and after 72 h the cells were used to the indicated experiments.

The mouse embryonic fibroblasts (MEFs) grow in Dulbecco's modified Eagle medium (DMEM) (Gibco) with addition of 1% penicillin/streptomycin, 1% non-essential amino acids solution, L-glutammine and 10% FBS at 37 °C with 5% CO_2 atmosphere.

Mfn2 KO MEFs were provided by Dr. Luca Scorrano, Department of Biology, University of Padova. $Parkin^{Flx/Flx}$ MEF were obtained from Dr. Ted Dawson, Johns Hopkins University [31]. TransFectin™ Lipid Reagent (Bio-Rad) or GenJet™ In Vitro DNA Transfection Reagent (SignaGen laboratories) were used for the transfection following the manufacturer's instruction. The medium was changed after 5 h and the experiments performed after 24 h/48 h from the transfection.

Human fibroblasts from skin biopsy were obtained from B.A., a 55-year old man who was diagnosed with PD at the age of 28 and presented an excellent response to a combination of levodopa and dopamine agonists until 2008. He then started complaining about motor fluctuations and involuntary movements and more recently developed pathological gambling, excessive impulsivity, aggressiveness and substance abuse (mainly cocaine). Cognitive testing in 2016 showed abnormalities in frontal executive and attention domains. His MRI revealed modest cortical and subcortical atrophy. Cells were grown in Dulbecco's modified Eagle medium (DMEM) (Gibco) with addition of 1% penicillin/streptomycin, 1% non-essential amino acids solution, L-glutammine and 10% FBS at 37 °C with 5% CO_2 atmosphere. Cells were used between passage P = 4 to P = 7 and transfection was performed using Lipofectamine Transfection Reagent (Invitrogen) achieving a maximal efficiency of transfection of 5%. For calcium measurement experiments, human fibroblasts were seeded onto 13 mm-diameter glass coverslips and maintained at 37 °C in a humidified incubator. After 24 h, cells were infected with lentiviral (LV) particles using the minimal dilution adequate for obtaining ≈70% of infected cells. Ca^{2+} measurements were performed 96 h after plating as described.

HEK-293 T cells to generate Lentiviral (LV) particles were grown in Dulbecco's modified Eagle's medium/High-Glucose (Euroclone), supplemented with 10% fetal bovine serum (Euroclone), 100 U/ml penicillin and 100 µg/ml streptomycin (Euroclone), and maintained at 37∘C in a humidified incubator with 5% CO_2

4.2. Lentiviral production and cell transduction

$[Ca^{2+}]_{cyt}$ and $[Ca^{2+}]_{mit}$ fluctuations analysis were performed by transducing human fibroblasts with a third generation lentivirus-based system that allow the expression of a chimeric construct encoding the Ca^{2+}-probe aequorin (AEQ) tagged with the influenza virus hemagglutinin (HA) epitope, and linked to sequences addressing the protein to the bulk cytosol (AEQcyt [70]) and mitochondrial matrix (AEQmit [71]), respectively. The transgene plasmids (pLV-AEQmit and pLV-AEQcyt) codifying for AEQmit and AEQcyt were generated by using an AEQ mutant with reduced Ca^{2+} affinity allowing $[Ca^{2+}]$ measurements up to hundreds of µM [72], while a chimeric construct of WT AEQ was used to generate the lentiviral vector for AEQcyt [73].

To obtain lentiviral particles, HEK-293 T cells were seeded onto 100 mm-diameter Petri dishes at ~40% confluence. 24 h after plating, cells were co-transfected, by means of calcium-phosphate procedure, with one of the transgene plasmids (pLV-AEQmit or pLV-AEQcyt) and

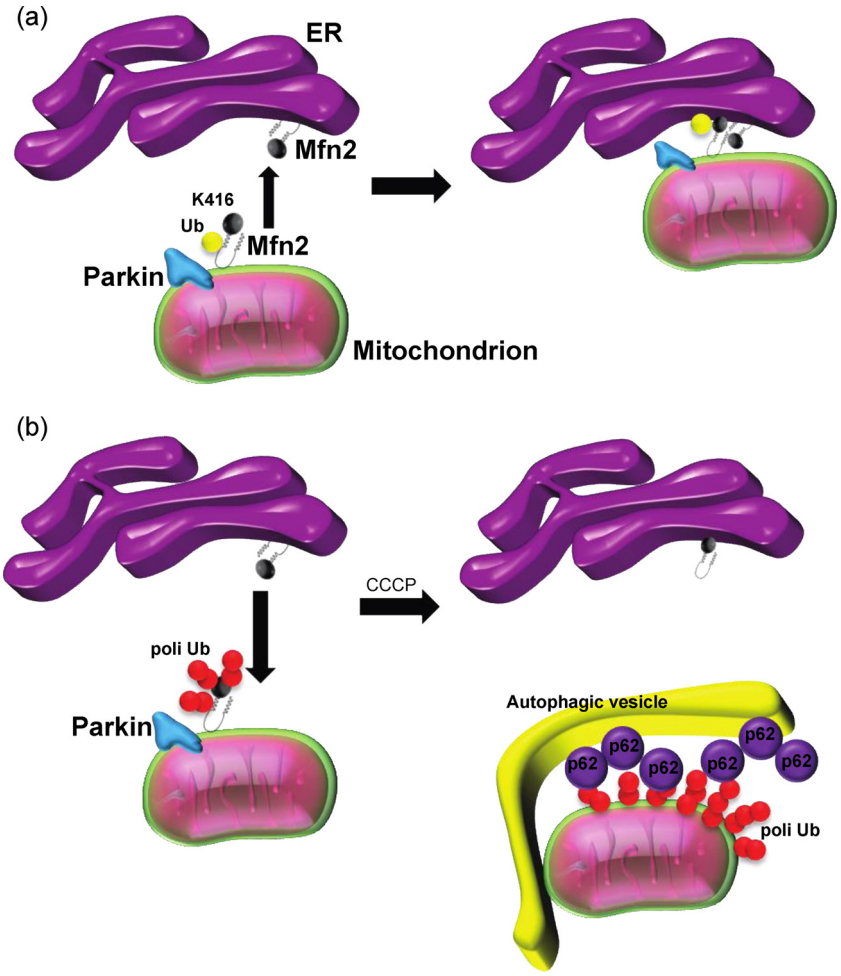

Fig. 6. Regulation of ER-mitochondria interaction by Parkin via Mfn2: a schematic representation.
Parkin ubiquitinates Mfn2 on lysine K416. This event is a prerequisite for ER-mitochondria physical and functional interaction (a). This model does not exclude the existence of a parallel pathway, which promotes Parkin-dependent ubiquitination of Mfn2, and additional OMM resident proteins, to promote mitophagy (b).

Table 1
Primers used for Site directed mutagenesis. Underscores indicate mismatch.

Constructs	Primers
Myc-Mfn2^{P251A}	Forward: 5‘-GCGTCTCTCCCGGGCAAACATCTTCATC-3‘
	Reverse: 5‘-GATGAAGATGTTTGCCCGGGAGAGACGC-3‘
Myc-Mfn2^{R280H}	Forward: 5‘-CAGCACATGGAGCATTGTACCAGCTTCC-3‘
	Reverse: 5‘- GGAAGCTGGTACAATGCTCCATGTGCTG -3‘
Myc-Mfn2^{K416R}	Forward: 5‘-GAGCTCTTGGCTCAAGACTATAGGCTCCGAATTAAGCAGATTACG-3‘
	Reverse: 5‘-CGTAATCTGCTTAATTCGGAGCCTATAGTCTTGAGCCAAGAGCTC-3‘
MFN^{P251A} Flag	Forward: 5‘-TCGCAGAAGCTAAGCAAGGCCAACATCTTCATCCTGAAC-3‘
	Reverse: 5‘-GTTCAGGATGAAGATGTTGGCCTTGCTTAGCTTCTGCGA-3‘
MFN^{R280H} Flag	Forward: 5‘-AAGTCTCAGCACACGGAACACTGCATCGACTTCCTCACC-3‘
	Reverse: 5‘-GGTGAGGAAGTCGATGCAGTGTTCCGTGTGCTGAGACTT-3‘
MFN^{K36R} Flag	Forward: 5‘-TTTGTGCGCGCCAGGAGGAGGATCAACGATATC-3‘
	Reverse: 5‘-GATATCGTTGATCCTCCTCCTGGCGCGCACAAA-3‘
MFN^{K416R} Flag/MFN^{K416R} GFP	Forward: 5‘-GGTTACGCGGGAAATGAGGATGAGGATCCACAACATGGTCG-3‘
	Reverse: 5‘-CGACCATGTTGTGGATCCTCATCCTCATTTCCCGCGTAACC-3‘
MFN^{K737R} Flag	Forward: 5‘-AAGCTGCTCAGGAATAGGGCCGGTTGGTTGGAC-3‘
	Reverse: 5‘-GTCCAACCAACCGGCCCTATTCCTGAGCAGCTT-3‘

the packaging plasmids pMDLg/pRRE, pMD2.VSVG, pRSV-Rev. After 10 h, the transfection medium was replaced with fresh culture medium. After 72 h, the HEK-293 T culture medium was collected and viral particles were harvested by ultracentrifugation (50,000 × g, 2 h) and resuspended in phosphate buffered saline (PBS; 140 mM NaCl, 2 mM KCl, 1.5 mM KH2PO4, 8 mM Na2HPO4, pH 7.4). Lentiviral stock infectivity was estimated by anti-HA immunocytochemistry as described in Lazzari et al. [74]. All procedures for the production and use of lentiviral particles were performed in a biosafety level-2 environment.

4.3. Measurements of mitochondrial and cytosolic Ca^{2+} fluxes

Cells were incubated (1 h, 37∘C, 5% CO2) with the prosthetic group coelenterazine (5 μM, Santa Cruz Biotechnology, cat. n. sc-205904) in

$CaCl_2$-containing Krebs-Ringer buffer (KRB-$CaCl_2$, 125 mM NaCl, 1 mM Na_3PO_4, 1 mM $MgSO_4$, $CaCl_2$ 1 mM, 5.5 mM glucose, 5 mM KCl, 20 mM HEPES, pH 7.4) and then transferred to the recording chamber—-equipped with a perfusion system—located into the luminometer. For the measurements of $[Ca^{2+}]_{cyt}$ and $[Ca^{2+}]_{mit}$, after a 30 s-perfusion step with KRB-$CaCl_2$, fibroblasts were stimulated with a mixture of 100 μM ATP and 100 μM histamine dissolved in KRB-$CaCl_2$. The experiments were terminated by cell permeabilization with digitonin (100 μM, Sigma) in Ca^{2+}-rich solution (10 mM $CaCl_2$ in H_2O). AEQ light emission was collected by means of an in-house built luminometer, equipped with a low-noise photo-multiplier coupled by an A/D board to a computer-assisted acquisition system, with a 1 Hz sampling rate [75]. This allowed the calibration of the recorded light signal to the total AEQ content. Conversion of light signal into Ca^{2+} concentration was performed as described in Brini et al. [70] and Montero et al. [76].

4.4. Molecular biology

pEYFP-ER (ER YFP), mRFP, pCB6-Myc-Mfn2 (Mfn2 WT) were previously described (de Brito and Scorrano [8]). pcDNA 3.1 CRE (CRE), pcDNA 3.1 (Empty vector) and pcDNA 3.1 mitoKate were available in our lab. Site directed mutagenesis was performed from Myc-Mfn2 using QuikChange II XL Site-Directed Mutagenesis Kit (Agilent) to obtain Myc-Mfn2^{P251A} (Mfn2^{P251A}), Myc-Mfn2^{R280H} (Mfn2^{R280H}) and Myc-Mfn2^{K416R} (Mfn2^{K416R}) (primers in Table 1). pAct-PPA Marf-Flag (MFN) and pAct-PPA Marf GFP (MFN GFP) constructs were previously generated [19] and were available in the lab. Site directed mutagenesis was performed to generate MFN^{P251A} Flag, MFN^{R280H} Flag, MFN^{K36R} Flag, MFN^{K416R} Flag, MFN^{K737R} Flag, MFN^{K416R} GFP (primers in Table 1) using QuikChange II XL Site-Directed Mutagenesis Kit (Agilent). HA-Ubiquitin (HA-Ub) was obtained from Addgene. FRET based Mito-ER Linker probe (FEMP) and mitochondrial low-affinity aequorin (mtAEQ mut) were previously described [29,72].

4.5. Parkin siRNA and MFN RNAi treatment

Parkin siRNA was transfected using Oligofectamine™ reagent (Invitrogen) and 100 nM of siRNA for each treatment following manufacturer instructions. The same amount of scrambled siRNA was used as control. For Parkin knockdown, cells were incubated with siRNA for at least 48 h. For RNA interference, cells were transfected with Parkin siRNA HSS107593 (Invitrogen).

Double-stranded RNAs (dsRNAs) were prepared using the MEGAscript kit (Ambion) according to the manufacturer's instructions. Primers used to generate dsRNAs contained a T7 promoter sequence at the 5′ end (MFN forward primer 5′-GGAACCTCTTTATTCTCTAT-3′ and reverse primer 5′-GGTTTGCTTTGCCCCAACAT-3′). A total of 1 million S2R + cells were plated on a six-well plate and treated with 15 μg dsRNA probe in serum-free medium. One hour after probe treatment, complete medium was added to the wells, and cells were cultured for 2 days before being transfected.

4.6. RNA isolation and Real time PCR

Parkin$^{Flx/Flx}$ MEF cells were transfected with the pcDNA 3.1-CRE (CRE) or empty vector (CTRL) and after 48 h total RNA was extracted from the cells with TRIzol™ Reagent (Invitrogen™) according to the manufacturer's instructions. Two hundred and fifty ng of RNA was reverse transcribed with SensiFAST™ cDNA Synthesis Kit (Bioline). Briefly, GoTaq qPCR Master mix containing SYBR green fluorescent dye (Promega) was mixed with 1 μl cDNA and 0.2 μM primers: *Parkin* forward primer 5′-AGGAATGCGTGCTGCAAATG-3′, reverse primer 5′-CTGTAGGCCTGAGAAGTGGC-3′; *mRPL13 A* forward primer 5′-TGA AGCCTACCAGAAAGTTTGC-3′, reverse primer 5′−CCAGGAGTCCGTT GGTCTTG-3′ in a final volume of 10 μl. Each cycle consisted of denaturation at 95 °C for 15 s, annealing at 60 °C for 60 s and extension at 95 °C for 15 s. Reactions were carried out on the 7900 H T Fast Real-time PCR System (Applied Biosystems). Quantification of gene expression (Relative level) was performed according to the $2^{-\Delta CT}$ method using *mRPL13 A* gene as internal control. Reactions were run in triplicate (technical replicates) and three independent experiments were performed.

4.7. Immunoblotting

MEFs were washed with phosphate-buffered saline (PBS) and scraped off using plastic cell scraper in PBS. The cells were centrifuged at 3000 rpm at 4 °C for 5 min. The supernatant was discarded and the pellet resuspended in appropriate volume of modified RIPA buffer (50 mM Tris−HCl, pH 7.4; 1% TritonX; 0.5% Na-deoxycholate; 0.1% SDS; 150 mM NaCl; 2 mM EDTA; 50 mM NaF), upon addition of fresh protease Inhibitor Cocktails (PIC), 50μM MG132 and 10 mM *N*-Ethylmaleimide (NEM; a deubiquitinase inhibition). The cells were incubated in ice for 30 min. and vigorously mixed every 10 min. and were centrifuged at 4000 rpm for 10 min. at 4 °C and the supernatant was transferred to new tube.

SR2+ cells protein lysate was obtained following incubation with a buffer composed of: 50 mM Tris−HCl, 150 mM NaCl, 1% Triton X, 2 mM EGTA, 1 mM MgCl2 with in addition 10% glycerol, PIC (100X), 10 mM NEM and 50 μM MG132. Cells were centrifuged at 4000 rpm for 10 min. at 4 °C and the supernatant was transferred to new tube.

Protein content was quantified using the Pierce™ BCA Protein Assay Kit (Thermo Scientific™).

NuPAGE™ LDS Sample Buffer (4X) (Invitrogen™) and 2-Mercaptoethanol (SIGMA) were added to the samples and proteins were boiled at 95 °C for 10 min.. Proteins were loaded in ExpressPlus™ PAGE Gel,10 × 8, 8% (GenScript) or NuPAGE™ 3–8% Tris-Acetate Protein Gels, 1.0 mm (Invitrogen™) and separated using a constant voltage of 100 mV for the appropriate time. After electrophoresis run, proteins were transferred from the gel matrix to Polyvinylidene difluoride (PVDF) membrane (Thermo Fisher Scientific) applying a constant voltage of 100 mV for 2 h at 4 °C. The membrane was saturated upon incubation with 5% milk in T-BST (mixture of tris-buffered saline and Tween 20) for 1 h. Proteins were probed using the following antibodies: α-Flag (1:1000; Cell Signaling Technology: 2368S), α-Mfn2 (1:1000; Abnova: H00009927-M03), α-PINK1 (1:500; Novus Biologicals: BC100-494), α-HA (1:1000; Cell Signaling Technology: 3724).

4.8. Immunoprecipitation (IP)

MEFs (about 500 000 cells) were plated in a 100 mm dish and the day after were transfected with the Mfn2 WT or the Mfn2 mutants and HA-Ub. 12 or 24 h later, cells were lysed with a buffer composed of: 50 mM Tris−HCl, 150 mM NaCl, 1% Triton X, 2 mM EGTA, 1 mM MgCl2 with in addition 10% glycerol, PIC (100X), 10 mM NEM and 50μM MG132. Protein extract (250μg-1 mg) was incubated with 10 μl of protein A agarose beads (Roche), previously balanced in lysis buffer, for 30 min. at 4 °C on the wheel (pre-cleaning). In parallel 30 μl of balanced beads were incubated with 1 μg of α-Mfn2 (Abcam: ab56889) or without the antibody (negative control) for 1 h and half at 4 °C on wheel in 70 μl of lysis buffer. Pre-cleaning beads were centrifugated at 4000 rpm for 5 min. and the supernatant was incubated overnight at 4 °C with antibody-conjugated beads. The day after the mix was centrifugated and the supernatant was discarded. Beads were washed 3 times for 10 min. at 4 °C with lysis buffer and boiled for 10 min. at 95 °C in 30–50 μl Laemmli loading buffer 2X (Laemmli 4X: Tris HCL 300 μM, pH 6.8; SDS 300 μM; Sucrose 1,4 M; Beta mercaptoethanol 8%; + Bromophenol blue). Supernatant was recovered upon maximum speed centrifugation and analyzed by western blotting in NuPAGE™ 3–8% Tris-Acetate Protein Gels.

4.9. Imaging acquisition and processing

MEFs or S2R + cells were plated on 24 mm round glass coverslips and co-transfected with mitoKate or mito-RFP and ER-YFP and the indicated plasmids for 48–72 h before imaging. Images were acquired using an UPlanSApo 60X/1.35 objective (iMIC Adromeda) upon excitation with 561 and 488 lasers. The percentage of ER that colocalize with mitochondria was measured with Mander's coefficient of colocalization (JACoP), following 3D volume rendered reconstruction of 60 z-axis images separated by 0.2 μm (software: imageJ, plug in: volumeJ).

For FRET imaging about 1200–1800 MEFs cells were seeded on 384 well plate (Perkin Elmer). After 12 h cells were transfected with FEMP probe and the indicated plasmids (ratio 1:3) using Genjet in Vitro DNA Transfection Reagent and analyzed using Perkin Elmer Operetta High-Content Imaging System objective 20X after 12 or 24 h. FEMP probe is targeted to the mitochondrial outer membrane (OMM) (targeting sequence mAKAP1 connected to YPF fluorescent protein) and ER (targeting sequence Sac1 connected to CFP fluorescent protein) and contains a self-leaving Tav2 A peptide, which undergoes autocleavage releasing YFP and CFP. FRET intensity is inversely proportional to the distance between the two fluorophores that are appropriately targeted to the two compartments. In the FEMP probe, OMM and ER targeting sequence are coupled with the two components of the FKBP-FRP heterodimerization system that allows covalent linkage between ER and mitochondria upon rapamycin administration. ER-mitochondria juxtaposition can therefore be correlated to FRET intensity and rapamycin treatment allows heterodimerization between adjacent FKBP and FRB domains to maximize FRET intensity. The basal FRET level (FRET basal) was obtained using ex 410–430 and em 460–500 for CFP and ex 490–510 and em 520–560 for YFP while YFP_{FRET} was obtained using ex 410–430 and em 520–560. The maximum FRET intensity (FRETmax) was measured after treatment with 100 μM Rapamycin for 15 min, on fixed cells in PBS (1% Formaldehyde for 10 min.). The images were analyzed using Perkin Elmer Harmony 3.5 image software. The YFP channel was used to mark the ROI (Fcell) and a second bonder, around each ROI, was plotted to measure and subtract the background intensity (Fbg). FRETbasal and FRETmax were calculated as: FYFPF-RETcell-FYFPFRETbg)/(FCFPcell-FCFPbg). The FRET Ratio (ΔR/R) is (FRETmax-FRETbasal)/FRETbasal. For FRET imaging of the human fibroblasts about 1800 cells were seeded on 384 well plate (Perkin Elmer). After 24 h cells were transfected with FEMP using Transfection Reagent PEI and analyzed using Perkin Elmer Operetta High-Content Imaging System objective 20X after 12 h.

Human fibroblast from skin biopsy (50.000 cells) were plated on 24 mm round glass coverslips and after 12 h for mitochondria analysis the cells were treated with 1 μ M of Tetramethylrhodamine methyl ester (TMRM) and 10 nM cyclosporin H in HBSS for 20 min. at 37 °C or transfected with ER-YFP for 12 h with PEI for ER analysis. Images were acquired using an UPlanSApo 40X/1.00 objective (iMIC Adromeda) upon excitation with 561 or 488 lasers. The 60 z-axis images separated by 0.2 μm were analysis using Volocity 6.3 software to obtain quantitative analysis of the mitochondrial volume, surface area, skeletal length, skeletal diameter. The number of cells per genotype that have been assessed for morphological analysis is minimum 200 per genotype and the average number of mitochondria that have been analysed is 50 per cell. The aspect ratio (AR) was calculated by dividing the mitochondrial skeletal length by the mitochondrial skeletal diameter.

4.10. Bioinformatic analysis

Protein sequences of MFN2_HUMAN (O95140), MFN2_MOUSE (Q80U63) and MARF_DROME (Q7YU24) were obtained from database Protein (UniProt). The alignment was performed using MultAlin software.

4.11. Aequorin measurement

MEFs were grown on 13 mm round glass coverslips at 50–60% of confluence and co-transfected with the indicated constructs and mitochondrial low affinity aequorin (mtAEQ mut). Cells were incubated for 1.5 h at 37 °C in DMEM 1% FBS after being reconstituted with 5 μM coelenterazine wt (invitrogene). To monitor mitochondrial Ca^{2+} transients, cells were perfused with Krebs Ringer buffer (KRB: 125 mM NaCl, 5 mM KCl, 1 mM Na_3PO_4, 1 mM $MgSO_4$, 5.5 mM glucose, 20 mM HEPES, pH 7.4, 37 °C, 1 Mm $CaCl_2$) for 20–30 s with or without 200 μM ATP. At the end of each experiment, the cells are perfused with milliQ H_2O_2 containing 10 mM $CaCl_2$ and 100 μM digitonin to calibrate the luminescence signal in Ca^{2+} values. The rate of Ca^{2+} uptake is calculated as Ca^{2+} uptake speed in μM/s at the half of peak upon treatment with 200 μM ATP.

4.12. Electron microscopy

Cells cultured in 24 well plate were fixed in 2% paraformaldehyde, 2.5% gluteraldehyde for 1 h/overnight. After rinsing in 0.1 M cacodylate buffer with 1% tannic acid, samples were post-fixed in 1:1 2% OsO_4 and 0.2 M cacodylate buffer for 1 h. Samples were rinsed, dehydrated in an ethanol, and embedded by using Epon. Ultrathin sections were examined using a transmission electron microscope. The number of contacts that have been analysed for ultrastructure is a minimum of 200 contacts per condition.

4.13. Fly stocks and breeding condition

Fly lines were grown on standard cornmeal medium and were maintained at 23 °C, 70% relative humidity, on a 12-h light:12-h dark cycle. The UAS mitoGFP/TM6B and UAS KDELGFP/TM6B were obtained from the lab of Prof. Daga, Department of Pharmaceutical and Pharmacological Sciences, University of Padova. The mito-ER syntetic linker, created by Csordás, consists of a monomeric fluorescent protein (mRFP) fused to the OMM targeting sequence of mAKAP1 at the N terminus and fused to the ER targeting sequence of yUBC6 at the C terminus [43]. The construct was cloned into a fly vector (pUAST) and two fly lines expressing different levels of the tethering construct were generated by random insertion into a *white1118*$^{-}$ background or PINK1 mutant (KO) background ($PINK1^{B9}$/FM7): UAS-mito-mRFP-ER^{TH}/TM6B (TH, high expression of tether) and UAS-mito-mRFP-$ER^{™}$/TM6B (TM, mild expression of tether). In order to activate neuronal expression of the tethering construct, flies were crossed with nSyb-Gal4/TM6B, neuronal Synaptobrevin-expressing flies obtained from the Bloomington stock center. PINK1 mutant (KO) flies (PINK1B9/FM7) [24] were a kind gift of Dr. Alexander Whitworth.

4.14. Mounting and imaging of fly wing

Flies at 3–5 days of age were fixed with 4% of paraformaldehyde (PFA) for 2 h at room temperature on a rotating wheel and then washed 3 times for 10 min with PBS. The whole wings were cut with Castro-Viejo Scissors, mounted on 24 mm round glass coverslips with a small amount of ProLong™ Gold Antifade Mountant and subsequently covered with another 12 mm round glass coverslip which was fixed with nail polish. The images were acquired using an UPlanSApo 20X/0.75 objective (iMIC Adromeda) after the excitation with a 561 laser. The quantification of the RFP signal was performed counting the spots using ImageJ along 150 μm of length of the L1 vein neural bundle [48] from the intersection of the L2 vein to proximal side of the wing flies.

4.15. Climbing assay

The climbing test was performed at 3 days of age at the same time of the day with male flies of the indicated genotypes. 10 flies for each

genotype were transferred in a plastic cylinder of 12 cm of length and 5 cm of diameter, marked with a line at 6 cm from the bottom of the tube. Flies were tapped to the bottom of the tube and the number of flies that successfully climbed across the 6 cm line in 10 s was counted. Fifteen separate and consecutive trials were performed for each experiment, and the results were averaged. 50 flies for each genotype were analyzed. The results were expressed as percentage of climbing flies.

4.16. Eggs-to-adults viability

The assay was performed to analyze eggs-to-adults viability of the tethering TM and TH flies compared to WT flies. For each lines (WT, WT TM and WT TH) 10 virgin females were crossed with 10 males nSyb-Gal4/TM6B on a plate with sugar yeast fruit medium. The day after, adults were removed and after 3 days eggs were counted. Next the medium with eggs was added to the tube with standard cornmeal medium. After 5 and 10 days from egg laying, the number of pupae and the number of male adults were counted. To analyze the eggs-to-pupae viability the number of pupae was divided by the number of eggs for each genotype and the resulting value was normalized to control (WT). In order to address the larvae-to-adults viability, the number of male adults was divided by the total number of pupae and expressed as percentage.

4.17. Statistics

Data were presents as mean ± SEM from at least three independent experiments. Statistical significance was determined using Unpaired *t*-test and p values are indicated (GraphPad software).

Author contribution

VB and EM designed, performed and interpreted experiments; CP performed calcium measurement experiments in patient fibroblasts; JC performed some of the western blotting; SVS designed and performed *in vivo* experimental work in flies and data analysis; MG performed some of the FEMP experiments and analysed FRET data analysis; DO performed calcium measurement experiments in MEFs; VD generated the tethering *Drosophila* fly lines; FC performed electron microscopy acquisition and provide technical support; ET and VP generated and maintained primary human fibroblasts from skin biopsy; CA, AA, AB and MB critically read the manuscript and conceptually contributed to manuscript content. EZ conceived and supervised the project, designed and interpreted experiments and wrote the manuscript.

Declaration of interests

None.

Acknowledgements

This work was supported by grants from Italian Ministry of Health “Ricerca Finalizzata” [GR-2011-02351151], Rita Levi Montalcini “Brain Gain” program and Michael J. Fox RRIA 2014 [Grant ID 9795] to E.Z. We also thank PISCOPIA-MARIE CURIE fellowship for the support. We would like to acknowledge Francesco Boldrin from the EM facility for their help and technical support. We are grateful to Emilie Schrepfer for her help with the graphical modelling of Fig. 6. We are also deeply grateful to Professor Luca Scorrano for his intellectual contribution and for critically reading the manuscript.

Appendix A. Supplementary data

Supplementary material related to this article can be found, in the online version, at doi:https://doi.org/10.1016/j.phrs.2018.09.006.

References

[1] B. Thomas, M.F. Beal, Parkinson’s disease, Hum. Mol. Genet 16 (2007) R183–194, https://doi.org/10.1093/hmg/ddm159 Spec No. 2.
[2] V. Bogaerts, J. Theuns, C. van Broeckhoven, Genetic findings in Parkinson’s disease and translation into treatment: a leading role for mitochondria? Genes Brain Behav. 7 (2008) 129–151, https://doi.org/10.1111/j.1601-183X.2007.00342.x.
[3] J. Bereiter-Hahn, M. Voth, Dynamics of mitochondria in living cells: shape changes, dislocations, fusion, and fission of mitochondria, Microsc. Res. Technol. 27 (1994) 198–219, https://doi.org/10.1002/jemt.1070270303.
[4] M. Rojo, F. Legros, D. Chateau, A. Lombes, Membrane topology and mitochondrial targeting of mitofusins, ubiquitous mammalian homologs of the transmembrane GTPase Fzo, J. Cell Sci. 115 (2002) 1663–1674.
[5] E.D. Wong, et al., The dynamin-related GTPase, Mgm1p, is an intermembrane space protein required for maintenance of fusion competent mitochondria, J. Cell. Biol. 151 (2000) 341–352.
[6] S. Cipolat, O. Martins de Brito, B. Dal Zilio, L. Scorrano, OPA1 requires mitofusin 1 to promote mitochondrial fusion, Proc. Natl. Acad. Sci. U. S. A. 101 (2004) 15927–15932, https://doi.org/10.1073/pnas.0407043101.
[7] Y. Chen, et al., Mitofusin 2-containing mitochondrial-reticular microdomains direct rapid cardiomyocyte bioenergetic responses via interorganelle Ca(2+) crosstalk, Circ. Res. 111 (2012) 863–875, https://doi.org/10.1161/CIRCRESAHA.112.266585.
[8] O.M. de Brito, L. Scorrano, Mitofusin 2 tethers endoplasmic reticulum to mitochondria, Nature 456 (2008) 605–610.
[9] P. Cosson, A. Marchetti, M. Ravazzola, L. Orci, Mitofusin-2 independent juxtaposition of endoplasmic reticulum and mitochondria: an ultrastructural study, PloS One 7 (2012) e46293, , https://doi.org/10.1371/journal.pone.0046293.
[10] R. Filadi, et al., Mitofusin 2 ablation increases endoplasmic reticulum-mitochondria coupling, Proc. Natl. Acad. Sci. U. S. A. 112 (2015) E2174–2181, https://doi.org/10.1073/pnas.1504880112.
[11] A.A. Rowland, G.K. Voeltz, Endoplasmic reticulum-mitochondria contacts: function of the junction, Nat. Rev. Mol. Cell Biol. 13 (2012) 607–625, https://doi.org/10.1038/nrm3440.
[12] R. Rizzuto, et al., Close contacts with the endoplasmic reticulum as determinants of mitochondrial Ca2+ responses, Science 280 (1998) 1763–1766.
[13] J.E. Vance, Phospholipid synthesis in a membrane fraction associated with mitochondria, J. Biol. Chem. 265 (1990) 7248–7256.
[14] T. Cali, D. Ottolini, A. Negro, M. Brini, Enhanced Parkin levels favor ER-mitochondria crosstalk and guarantee Ca(2+) transfer to sustain cell bioenergetics, Biochim. Biophys. Acta 1832 (2013) 495–508, https://doi.org/10.1016/j.bbadis.2013.01.004.
[15] D. Ottolini, T. Cali, A. Negro, M. Brini, The Parkinson disease-related protein DJ-1 counteracts mitochondrial impairment induced by the tumour suppressor protein p53 by enhancing endoplasmic reticulum-mitochondria tethering, Hum. Mol. Genet 22 (2013) 2152–2168, https://doi.org/10.1093/hmg/ddt068.
[16] T. Cali, D. Ottolini, A. Negro, M. Brini, Alpha-synuclein controls mitochondrial calcium homeostasis by enhancing endoplasmic reticulum-mitochondria interactions, J. Biol. Chem. 287 (2012) 17914–17929, https://doi.org/10.1074/jbc.M111.302794.
[17] A.V. Panov, et al., Early mitochondrial calcium defects in Huntington’s disease are a direct effect of polyglutamines, Nat. Neurosci. 5 (2002) 731–736, https://doi.org/10.1038/nn884.
[18] D. Narendra, A. Tanaka, D.F. Suen, R.J. Youle, Parkin is recruited selectively to impaired mitochondria and promotes their autophagy, J. Cell. Biol. 183 (2008) 795–803.
[19] E. Ziviani, R.N. Tao, A.J. Whitworth, Drosophila parkin requires PINK1 for mitochondrial translocation and ubiquitinates mitofusin, Proc. Natl. Acad. Sci. U. S. A. 107 (2010) 5018–5023, https://doi.org/10.1073/pnas.0913485107.
[20] A.C. Poole, et al., The PINK1/Parkin pathway regulates mitochondrial morphology, Proc. Natl. Acad. Sci. U. S. A. 105 (2008) 1638–1643.
[21] A. Tanaka, et al., Proteasome and p97 mediate mitophagy and degradation of mitofusins induced by Parkin, J. Cell. Biol. 191 (2010) 1367–1380.
[22] M.E. Gegg, et al., Mitofusin 1 and mitofusin 2 are ubiquitinated in a PINK1/Parkin-dependent manner upon induction of mitophagy, Hum. Mol. Genet 19 (2010) 4861–4870, https://doi.org/10.1093/hmg/ddq419.
[23] I.E. Clark, et al., Drosophila pink1 is required for mitochondrial function and interacts genetically with Parkin, Nature 441 (2006) 1162–1166.
[24] J. Park, et al., Mitochondrial dysfunction in Drosophila PINK1 mutants is complemented by Parkin, Nature 441 (2006) 1157–1161.
[25] Y. Yang, et al., Mitochondrial pathology and muscle and dopaminergic neuron degeneration caused by inactivation of Drosophila Pink1 is rescued by parkin, Proc. Natl. Acad. Sci. U. S. A. 103 (2006) 10793–10798.
[26] N. Exner, et al., Loss-of-function of human PINK1 results in mitochondrial pathology and can be rescued by Parkin, J. Neurosci. 27 (2007) 12413–12418, https://doi.org/10.1523/JNEUROSCI.0719-07.2007.
[27] F. Anton, G. Dittmar, T. Langer, M. Escobar-Henriques, Two deubiquitylases act on mitofusin and regulate mitochondrial fusion along independent pathways, Mol. Cell. 49 (2013) 487–498, https://doi.org/10.1016/j.molcel.2012.12.003.
[28] V. Debattisti, D. Pendin, E. Ziviani, A. Daga, L. Scorrano, Reduction of endoplasmic reticulum stress attenuates the defects caused by drosophila mitofusin depletion, J. Cell. Biol. 204 (2014) 303–312, https://doi.org/10.1083/jcb.201306121.
[29] D. Naon, et al., Critical reappraisal confirms that Mitofusin 2 is an endoplasmic reticulum-mitochondria tether, Proc. Natl. Acad. Sci. U. S. A. 113 (2016) 11249–11254, https://doi.org/10.1073/pnas.1606786113.

[30] J.H. Shin, et al., PARIS (ZNF746) repression of PGC-1alpha contributes to neurodegeneration in Parkinson's disease, Cell 144 (2011) 689–702, https://doi.org/10.1016/j.cell.2011.02.010.

[31] R. Von Coelln, et al., Loss of locus coeruleus neurons and reduced startle in parkin null mice, Proc. Natl. Acad. Sci. U. S. A. 101 (2004) 10744–10749, https://doi.org/10.1073/pnas.0401297101.

[32] S. Zuchner, et al., Mutations in the mitochondrial GTPase mitofusin 2 cause Charcot-Marie-Tooth neuropathy type 2A, Nat. Genet 36 (2004) 449–451, https://doi.org/10.1038/ng1341.

[33] H. Chen, et al., Mitofusins Mfn1 and Mfn2 coordinately regulate mitochondrial fusion and are essential for embryonic development, J. Cell. Biol. 160 (2003) 189–200, https://doi.org/10.1083/jcb.200211046.

[34] S. Mattie, J. Riemer, J.G. Wideman, H.M. McBride, A new mitofusin topology places the redox-regulated C terminus in the mitochondrial intermembrane space, J. Cell. Biol. 217 (2018) 507–515, https://doi.org/10.1083/jcb.201611194.

[35] M.M. Cohen, G.P. Leboucher, N. Livnat-Levanon, M.H. Glickman, A.M. Weissman, Ubiquitin-proteasome-dependent degradation of a mitofusin, a critical regulator of mitochondrial fusion, Mol. Biol. Cell 19 (2008) 2457–2464, https://doi.org/10.1091/mbc.E08-02-0227.

[36] A. Rakovic, et al., Mutations in PINK1 and Parkin impair ubiquitination of mitofusins in human fibroblasts, PloS One 6 (2011) e16746, , https://doi.org/10.1371/journal.pone.0016746.

[37] B. Bingol, et al., The mitochondrial deubiquitinase USP30 opposes Parkin-mediated mitophagy, Nature 510 (2014) 370–375, https://doi.org/10.1038/nature13418.

[38] S.A. Sarraf, et al., Landscape of the PARKIN-dependent ubiquitylome in response to mitochondrial depolarization, Nature 496 (2013) 372–376, https://doi.org/10.1038/nature12043.

[39] G. Xu, S.R. Jaffrey, Proteomic identification of protein ubiquitination events, Biotechnol. Genetic Eng. Rev. 29 (2013) 73–109, https://doi.org/10.1080/02648725.2013.801232.

[40] S. Paillusson, et al., There's something wrong with my MAM; The ER-mitochondria axis and neurodegenerative diseases, Trends Neurosci. 39 (2016) 146–157, https://doi.org/10.1016/j.tins.2016.01.008.

[41] M. Krols, et al., Mitochondria-associated membranes as hubs for neurodegeneration, Acta Neuropathol. 131 (2016) 505–523, https://doi.org/10.1007/s00401-015-1528-7.

[42] C.S. Chan, et al., 'Rejuvenation' protects neurons in mouse models of Parkinson's disease, Nature 447 (2007) 1081–1086, https://doi.org/10.1038/nature05865.

[43] G. Csordas, et al., Structural and functional features and significance of the physical linkage between ER and mitochondria, J. Cell. Biol. 174 (2006) 915–921, https://doi.org/10.1083/jcb.200604016.

[44] G. Csordas, et al., Imaging interorganelle contacts and local calcium dynamics at the ER-mitochondrial interface, Mol. Cell. 39 (2010) 121–132, https://doi.org/10.1016/j.molcel.2010.06.029.

[45] D.P. Narendra, et al., PINK1 is selectively stabilized on impaired mitochondria to activate Parkin, PLoS Biol. 8 (2010) e1000298, , https://doi.org/10.1371/journal.pbio.1000298.

[46] B. Heeman, et al., Depletion of PINK1 affects mitochondrial metabolism, calcium homeostasis and energy maintenance, J. Cell Sci. 124 (2011) 1115–1125, https://doi.org/10.1242/jcs.078303.

[47] A. Sandebring, et al., Parkin deficiency disrupts calcium homeostasis by modulating phospholipase C signalling, FEBS J. 276 (2009) 5041–5052, https://doi.org/10.1111/j.1742-4658.2009.07201.x.

[48] A. Vagnoni, S.L. Bullock, A simple method for imaging axonal transport in aging neurons using the adult Drosophila wing, Nat. Protoc. 11 (2016) 1711–1723, https://doi.org/10.1038/nprot.2016.112.

[49] S. Gehrke, et al., PINK1 and Parkin control localized translation of respiratory chain component mRNAs on mitochondria outer membrane, Cell Metab. 21 (2015) 95–108, https://doi.org/10.1016/j.cmet.2014.12.007.

[50] A.K. Muller-Rischart, et al., The E3 ligase Parkin maintains mitochondrial integrity by increasing linear ubiquitination of NEMO, Mol. Cell. 49 (2013) 908–921, https://doi.org/10.1016/j.molcel.2013.01.036.

[51] N. Matsuda, et al., Diverse effects of pathogenic mutations of Parkin that catalyze multiple monoubiquitylation in vitro, J. Biol. Chem. 281 (2006) 3204–3209, https://doi.org/10.1074/jbc.M510393200.

[52] C. Hampe, H. Ardila-Osorio, M. Fournier, A. Brice, O. Corti, Biochemical analysis of Parkinson's disease-causing variants of Parkin, an E3 ubiquitin-protein ligase with monoubiquitylation capacity, Hum. Mol. Genet 15 (2006) 2059–2075, https://doi.org/10.1093/hmg/ddl131.

[53] K.L. Lim, et al., Parkin mediates nonclassical, proteasomal-independent ubiquitination of synphilin-1: implications for Lewy body formation, J. Neurosci. 25 (2005) 2002–2009, https://doi.org/10.1523/JNEUROSCI.4474-04.2005.

[54] L. Glauser, S. Sonnay, K. Stafa, D.J. Moore, Parkin promotes the ubiquitination and degradation of the mitochondrial fusion factor mitofusin 1, J. Neurochem. 118 (2011) 636–645, https://doi.org/10.1111/j.1471-4159.2011.07318.x.

[55] A.C. Poole, R.E. Thomas, S. Yu, E.S. Vincow, L. Pallanck, The mitochondrial fusion-promoting factor mitofusin is a substrate of the PINK1/Parkin pathway, PloS One 5 (2010) e10054, , https://doi.org/10.1371/journal.pone.0010054.

[56] I.H. Henn, et al., Parkin mediates neuroprotection through activation of IkappaB kinase/nuclear factor-kappaB signaling, J. Neurosci. 27 (2007) 1868–1878, https://doi.org/10.1523/JNEUROSCI.5537-06.2007.

[57] L. Fallon, et al., A regulated interaction with the UIM protein Eps15 implicates parkin in EGF receptor trafficking and PI(3)K-Akt signalling, Nat. Cell Biol. 8 (2006) 834–842, https://doi.org/10.1038/ncb1441.

[58] E.W. Doss-Pepe, L. Chen, K. Madura, Alpha-synuclein and Parkin contribute to the assembly of ubiquitin lysine 63-linked multiubiquitin chains, J. Biol. Chem. 280 (2005) 16619–16624, https://doi.org/10.1074/jbc.M413591200.

[59] L. Salmena, P.P. Pandolfi, Changing venues for tumour suppression: balancing destruction and localization by monoubiquitylation, Nat. Rev. Cancer 7 (2007) 409–413, https://doi.org/10.1038/nrc2145.

[60] K.K. Dove, R.E. Klevit, Structural biology: Parkin's serpentine shape revealed in the year of the snake, Curr. Biol.: CB 23 (2013) R691–693, https://doi.org/10.1016/j.cub.2013.07.039.

[61] T. Wauer, D. Komander, Structure of the human Parkin ligase domain in an autoinhibited state, EMBO J. 32 (2013) 2099–2112, https://doi.org/10.1038/emboj.2013.125.

[62] M. Hamasaki, et al., Autophagosomes form at ER-mitochondria contact sites, Nature 495 (2013) 389–393, https://doi.org/10.1038/nature11910.

[63] D. De Stefani, A. Raffaello, E. Teardo, I. Szabo, R. Rizzuto, A forty-kilodalton protein of the inner membrane is the mitochondrial calcium uniporter, Nature 476 (2011) 336–340, https://doi.org/10.1038/nature10230.

[64] J.R. Friedman, et al., ER tubules mark sites of mitochondrial division, Science 334 (2011) 358–362, https://doi.org/10.1126/science.1207385.

[65] Y. Kirichok, G. Krapivinsky, D.E. Clapham, The mitochondrial calcium uniporter is a highly selective ion channel, Nature 427 (2004) 360–364, https://doi.org/10.1038/nature02246.

[66] T. Cali, D. Ottolini, M. Brini, Calcium and endoplasmic reticulum-mitochondria tethering in neurodegeneration, DNA Cell Biol. 32 (2013) 140–146, https://doi.org/10.1089/dna.2013.2011.

[67] S. Gandhi, et al., PINK1-associated Parkinson's disease is caused by neuronal vulnerability to calcium-induced cell death, Mol. Cell. 33 (2009) 627–638, https://doi.org/10.1016/j.molcel.2009.02.013.

[68] S. Gandhi, et al., Dopamine induced neurodegeneration in a PINK1 model of Parkinson's disease, PloS One 7 (2012) e37564, , https://doi.org/10.1371/journal.pone.0037564.

[69] C.A. Gautier, et al., Regulation of mitochondrial permeability transition pore by PINK1, Mol. Neurodegener. 7 (2012) 22, https://doi.org/10.1186/1750-1326-7-22.

[70] M. Brini, et al., Transfected aequorin in the measurement of cytosolic Ca2+ concentration ([Ca2+]c). A critical evaluation, J. Biol. Chem. 270 (1995) 9896–9903.

[71] R. Rizzuto, A.W. Simpson, M. Brini, T. Pozzan, Rapid changes of mitochondrial Ca2+ revealed by specifically targeted recombinant aequorin, Nature 358 (1992) 325–327, https://doi.org/10.1038/358325a0.

[72] J.M. Kendall, G. Sala-Newby, V. Ghalaut, R.L. Dormer, A.K. Campbell, Engineering the CA(2+)-activated photoprotein aequorin with reduced affinity for calcium, Biochem. Biophys. Res. Commun. 187 (1992) 1091–1097.

[73] D. Lim, et al., Calcium signalling toolkits in astrocytes and spatio-temporal progression of Alzheimer's disease, Curr. Alzheimer Res. 13 (2016) 359–369.

[74] C. Lazzari, et al., Cellular prion protein is implicated in the regulation of local Ca2+ movements in cerebellar granule neurons, J. Neurochem. 116 (2011) 881–890, https://doi.org/10.1111/j.1471-4159.2010.07015.x.

[75] D. Ottolini, T. Cali, M. Brini, Methods to measure intracellular Ca(2+) fluxes with organelle-targeted aequorin-based probes, Methods Enzymol. 543 (2014) 21–45, https://doi.org/10.1016/B978-0-12-801329-8.00002-7.

[76] M. Montero, et al., Monitoring dynamic changes in free Ca2+ concentration in the endoplasmic reticulum of intact cells, EMBO J. 14 (1995) 5467–5475.